ANNUAL REVIEWS

Annual Review of Materials Research

Layered Double Perovskites

Hayden A. Evans,[1,*] Lingling Mao,[2,*] Ram Seshadri,[2,3,4] and Anthony K. Cheetham[2,4,5]

[1]Center for Neutron Research, National Institute of Standards and Technology, Gaithersburg, Maryland 20899, USA; email: hayden.evans@nist.gov

[2]Materials Research Laboratory, University of California, Santa Barbara, California 93106, USA; email: seshadri@mrl.ucsb.edu

[3]Department of Chemistry and Biochemistry, University of California, Santa Barbara, California 93106, USA

[4]Materials Department, University of California, Santa Barbara, California 93106, USA

[5]Department of Materials Science and Engineering, National University of Singapore, Singapore 117575

Annu. Rev. Mater. Res. 2021. 51:351–80

First published as a Review in Advance on May 5, 2021

The *Annual Review of Materials Research* is online at matsci.annualreviews.org

https://doi.org/10.1146/annurev-matsci-092320-102133

*These authors contributed equally to this article

Keywords

perovskites, layered compounds, ordering, crystal structure

Abstract

Successful strategies for the design of crystalline materials with useful function are frequently based on the systematic tuning of chemical composition within a given structural family. Perovskites with the formula ABX_3, perhaps the best-known example of such a family, have a vast range of elements on *A*, *B*, and *X* sites, which are associated with a similarly vast range of functionality. Layered double perovskites (LDPs), a subset of this family, are obtained by suitable slicing and restacking of the perovskite structure, with the additional design feature of ordered cations and/or anions. In addition to inorganic LDPs, we also discuss hybrid (organic-inorganic) LDPs here, where the *A*-site cation is a protonated organic amine. Several examples of inorganic LDPs are presented with a discussion of their ferroic, magnetic, and optical properties. The emerging area of hybrid LDPs is particularly rich and is leading to exciting discoveries of new compounds with unique structures and fascinating optoelectronic properties. We provide context for what is important to consider when designing new materials and conclude with a discussion of future opportunities in the broad LDP area.

1. INTRODUCTION

Inorganic three-dimensional (3D) perovskites, which adopt the general formula ABX_3, have had a remarkable scientific history over almost the past 100 years (1), with uses as ferroelectrics such as $BiTiO_3$ (2, 3), superconductors such as $Ba(Pb,Bi)O_3$ (4) as well as the perovskite-derived $YBa_2Cu_3O_x$ (5), and $LaMnO_3$-based materials that exhibit colossal magnetoresistance (6, 7). In recent decades, the chemistry of such perovskites has been extended into the realm of hybrid perovskites in which the A cation is often replaced by an amine and/or the X site is occupied by an organic linker (8). Important examples of the latter class include the methylammonium (MA) lead halides, $(MA)PbX_3$ (9), and dimethylammonium (DMA) transition metal formates, $[(CH_3)_2NH_2]Zn^{II}(HCOO)_3$ (10), which exhibit a wide range of interesting electronic and optoelectronic properties.

One of the fascinating features of 3D perovskites is that they can often be prepared in the form of so-called double perovskites (11), wherein, most commonly, the B sites are occupied by two different metals in an alternating manner that resembles a rock salt structure. These have the general formula $A_2BB'X_6$. The mineral cryolite Na_3AlF_6 (more correctly, Na_2NaAlF_6), so important for the processing of aluminum, is an example. Another is Sr_2FeMoO_6, which has attracted a great deal of interest in the condensed matter physics community on account of the unusual magnetic and electronic properties arising from the alternation of the Fe^{III} and Mo^{V} ions (12). Again, we find analogs in the hybrid world, with recent reports of double perovskites such as $(MA)_2AgBiX_6$ (13). There are also double perovskites in which there are two different cations on the A sites, i.e., AAB_2X_6 (one example is $CaFeTi_2O_6$), as well as double-double perovskites of the general formula $AA'BB'X_6$, in which there are two types of cations that are ordered on both the A sites and the B sites. The first detailed report of the latter was $NaLaMgWO_6$ (14). Finally, there are both inorganic and hybrid 3D perovskites that contain two types of ordered X anions, such as $SrTaO_2N$ (15) and $(GA)_2Mn_2(HCOO)_{1.5}(H_2POO)_{1.5}$, where GA = guanidinium (16). These, too, can be considered as double perovskites. **Figure 1** displays schemes of the perovskite crystal structure and how some of the structures of interest here are derived thereof.

There is an extensive literature on two-dimensional (2D) layered inorganic perovskites with the general formula A_2BX_4, especially with X = oxygen. These are obtained by slicing the 3D perovskite and adding features that reduce the dimensionality. Classical examples include K_2NiF_4 (17) and the first high-temperature cuprate superconductors based on La_2CuO_4 (18). There are also compounds with two (or more) octahedral layers of general composition $A_{n+1}B_nX_{3n+1}$ ($n = 2$, 3, etc.), such as $Sr_3Ti_2O_7$, a member of the so-called Ruddlesden-Popper (RP) series of compounds (19). The other well-known family of layered perovskite phases is the Dion-Jacobson (DJ) series (20, 21). Within the hybrid halide world, these have been the subject of recent attention and were reviewed in this journal in 2018 (22).

The scope of this article is on compounds that combine reduced dimensionality with doubling. These layered double perovskites (LDPs), besides being 2D, display ordering of cations or anions on the A, B, and X sites, as discussed above for 3D systems. We restrict the discussion to compounds in which there is either full or substantial ordering on the appropriate A, B, or X sites. As with the 3D systems, there are more examples of inorganic LDPs than of hybrid ones, although both classes are relatively new. Interesting inorganic examples include $Cs_4CuSb_2Cl_{12}$ (23), $LaSr_2Mn_2O_7$ (24, 25), and Ba_2TaO_3N (26). We show that the area of hybrid LDPs is particularly rich and is leading to exciting discoveries of new compounds with unique structures and fascinating properties. For example, $(BA)_4AgBiBr_8$ and $(BA)_2CsAgBiBr_7$ (BA = butylammonium) were recently obtained by incorporating BA cations into the 3D double perovskite $Cs_2AgBiBr_6$ (27).

The first part of the review describes all-inorganic systems, focusing on compounds that exhibit properties that are uniquely determined by the nature of their structures. The second part

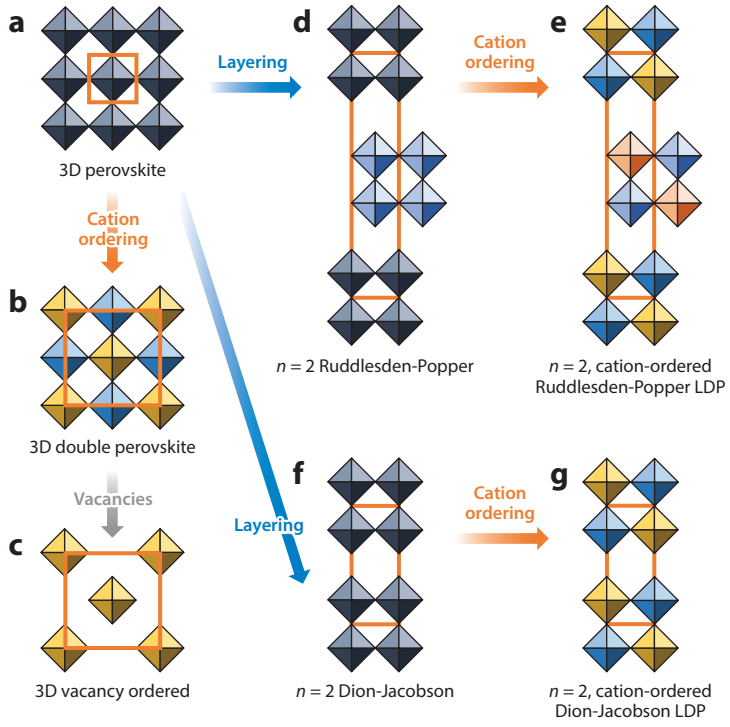

Figure 1

(*a*,*b*) Schemes displaying (*a*) octahedral connectivity and composition of the ABX_3 3D perovskite structure and (*b*) how forking of this structure through alternating the composition of cations on the *B* site in an ordered manner gives rise to the $BB'X_6$ 3D double perovskite. (*c*) If *B* sites are alternately skipped (left vacant), the structure of the 3D vacancy-ordered perovskite A_2BX_6 emerges. (*d*) The layered Ruddlesden-Popper structure with $n = 2$. (*e*) The Ruddlesden-Popper LDP formed through cation ordering. (*f*,*g*) Finally, schemes of the $n = 2$ Dion-Jacobson phase (*f*) without and (*g*) with cation ordering. The two LDPs are among the structure types emphasized here. For clarity, *A* species are not depicted. Abbreviation: LDP, layered double perovskite.

discusses hybrid compounds, including very recent examples that have both inorganic and organic cations on the *A* sites. The conclusion presents areas that are ripe for further exploration.

2. INORGANIC LAYERED DOUBLE PEROVSKITES

Inorganic LDPs are surprisingly numerous, given their strict definition. The group comprises predominantly pure oxides as well as many mixed anion phases (which understandably, are also largely oxide derived). The range of properties in these materials is quite diverse, spanning piezoelectrics (28), photocatalysts (29), ion conductors (30), thermometrics (31), and so on. There are also inorganic LDPs that are prime candidates for postsynthetic exfoliation to create nanosheets and heterostructures; this is a large area of research, and we direct interested readers to other sources (32–34).

The sections below are broadly ordered into doubling of the *A* or *B* sites (*AA′–B–X* or *A–BB′–X*), those with mixed anion sites (*A–B–XX′*), and finally combinations of each. These sections are also loosely ordered by increasing *n* (perovskite layer thickness), for which there are many examples. The compounds listed fall into three main structure types: RP, DJ (20, 21), and (111) layered perovskites. These phases have the following general formulas: RP = $A_{n+1}B_nX_{3n+1}$,

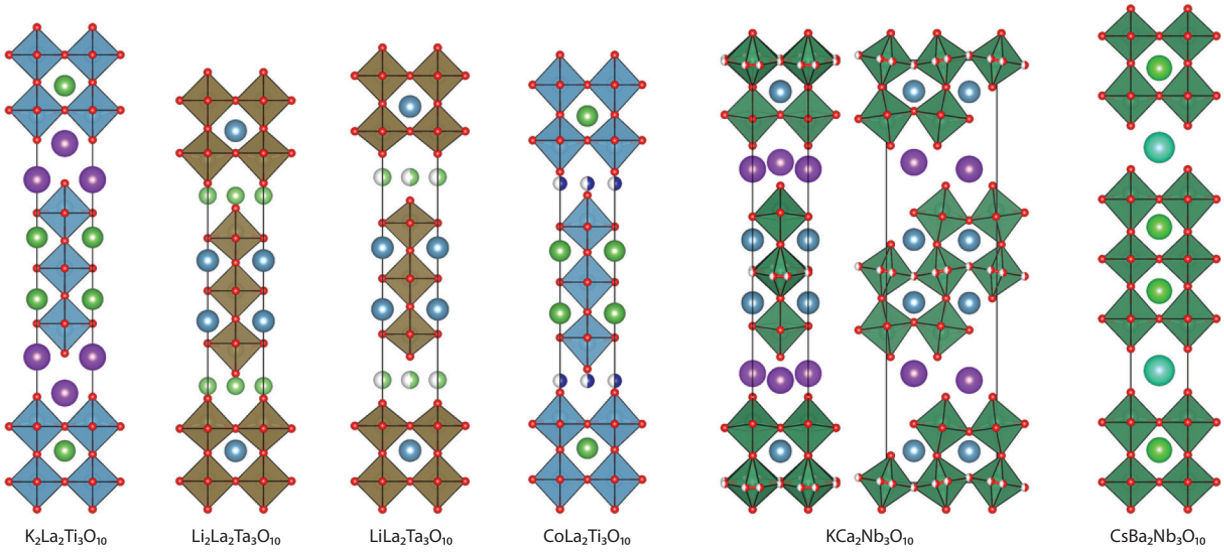

Figure 2

Depictions of various $n = 3$ compounds displaying a range of structure types, from Ruddleston-Popper to Dion-Jacobson, with examples of *A*-site ordering (35–39).

DJ = $A(A'_{n-1})B_nX_{3n+1}$, and (111) layered perovskites = $A_nB_{n-1}X_{3n}$. We note here that RP and DJ compounds are conventionally defined not only by the formula, but also by how the perovskite slabs arrange relative to each other. In the case of *A*-site ordering (**Figure 2**), one can see that the spectrum is nuanced. For this work, we use the information of perovskite slabs that are disposed relative to each other as the main indicator of whether it is a RP or a DJ, where RP perovskite slabs are staggered and DJ slabs are aligned.

The goal of Section 2 is not to provide an exhaustive list of LDPs, but instead to provide a concise survey of selected compounds that exemplify the possibilities. We discuss when one of the three possible structure types might be expected for a material and note how certain orderings of either the *A*, *B*, or *X* sites seem to encourage one of the three structural classes. These examples should provide design principles as to what elemental compositions are available if certain structures and symmetries are sought or, conversely, what structures are attainable if certain compositional orderings are desired.

2.1. Oxide Systems

Oxide LDPs present as any of the possible structure types [RP, DJ, and (111)], with *AA′*-site-ordered compounds being the most common. These compounds, owing to the −2 oxidation state of oxygen, have generally high oxidation state *B*-site metals (+3 through +7), which also accounts for the reduced variation and quantity of *B*-site-ordered compounds reported.

2.1.1. *AA′* oxide layered double perovskites. Much like the case of traditional perovskites (40), the charge difference of the select *A* and *A′* cations and, to a lesser extent, the radii of the cations need to be sufficiently different to achieve *A*-site ordering and to avoid disordering over the same sites. For example, $SrLa_2Sc_2O_7$, in which the ionic radii of Sr^{2+} and La^{3+} are 1.44 Å and 1.36 Å, respectively, is disordered. In terms of structure type, *A*-site-ordered LDPs form exclusively as either RP or DJ phases, with the final structure dictated by the ionic radii of the *A*-site cations

(41). For example, both $LiLaTiO_4$ and $KLaTiO_4$ are RPs, but how the two alkali metals order in each respective RP differs as a result of their ionic radii (coordination number = 8; ionic radii for Li and K are 0.92 Å and 1.51 Å, respectively) (42). This size variance and final ordering can play a role for certain materials, but in general there is not much difference in terms of properties between RP and DJ phases. However, one distinction is that RP phases generally have reduced interlayer spacings relative to DJ phases, and such reduced spacing can contribute to reduced interlayer ion mobilities (41) or reduced Brønsted acidity (43) or can impact long-range magnetic ordering.

The simplest family of oxide inorganic LDPs are the RP $AA'TiO_4$ compounds [A = H (44), Li (45, 46), Na (45), K (45, 47), Ag (48); A' = rare earths (49)], which have a structure related to the prototypical RP, K_2NiF_4. As mentioned above, A-site ordering differs depending on alkali metal ion size, which is a trend that continues in higher-n RP variants. The $AA'TiO_4$ compounds were examined in the 1990s as ion conductors ($NaLnTiO_4$) (50) and as photocatalysts (Zr-doped $KLaTiO_4$) (51), but recent research has focused on how these compounds are also piezoelectric; the compounds are rendered polar by long-overlooked symmetry-breaking octahedral rotations [$NaA'TiO_4$ (28) and $LiA'TiO_4$; A' = rare earths (52); $HA'TiO_4$ (53); $KA'TiO_4$ (54)]. The symmetry-breaking octahedral rotations were originally rationalized using Goldschmidt tolerance factors (1), but as theory indicated (via a study on $KA'TiO_4$), the octahedral rotation instability grows when the alkali ions become larger, which is in contrast to a simple tolerance factor argument (54). It has now been proposed that the primary driving force for the octahedral rotations in $KA'TiO_4$ is the need for optimized coordination environments for the rare-earth ions. The secondary driving force for the rotations is the interlayer lattice mismatch caused by the varying alkali metal ion sizes. Interestingly, the $AA'TiO_4$ compounds are the only $n = 1$ A-site-ordered oxide compounds, with the only similar compounds being ordered oxyanion phases, such as the recently reported Sr_2ScO_3Cl (55). These mixed oxyanion compounds are discussed in Section 2.3.

Similar to the $AA'TiO_4$ RP family are $n = 2$ compounds, such as $BaEu_2Mn_2O_7$ (56) and $Rb_2LaNb_2O_7$ (57). However, instead of the RP phases, we now draw attention to the DJ $AA'B_2O_7$ compounds (A = Rb, Cs; A' = rare earths, Bi; B = Nb, Ta), as they display emergent noncentrosymmetric behavior akin to the $n = 1$ $AA'TiO_4$ compounds (58). Although these and similar compounds have been known for some time [$RbLaNb_2O_7$ (57), $CsLaNb_2O_7$ (59), $RbLaTa_2O_7$ (60), $CsBiNb_2O_7$ (61, 62)], along with their (sometimes elusive) ferroelectric properties [$CsNdNb_2O_7$ and $CsBiNd_2O_7$] (63), there has been a renaissance in thinking as to why RP and DJ lower-dimensional compounds (not exclusively $n = 2$) are prime candidates for ferro/piezoelectric properties (64–67). Some illuminating cases include the DJ phases of $RbNdNb_2O_7$ and $RbNdTa_2O_7$—which can be Na or Li ion substituted to create RP analogs, where $LiNdB_2O_7$ is polar (68)—as well as the DJ phase $CsBiNb_2O_7$, which not only is a Rashba-Dresselhaus ferroelectric but also shows promise as a persistent spin helix material due to its lowered symmetry (69). Alternatively, oxide compounds have also been used as phosphors (60, 70), as shown for $ALa_{1-x}Ta_2O_7{:}xBi^{3+}$ (71, 72), photocatalysts such as $RbPb_2Nb_2O_7$ (29) and $Li_2CaTa_2O_7$ (73, 74), or even oxide ion conductors (as seen for $CsBi_2TiNbO_{10}$; the Ti and Nb are disordered) (75). However, as we discuss briefly below, the symmetry-breaking properties of these compounds are persistent, and even applications such as photocatalysis are impacted by induced dipoles brought about by the symmetry breaking.

The last part of this subsection focuses on the $n = 3$ compounds, as higher n values can exist but are much less common. The inherent properties of the $n = 3$ compounds remain closer to the $n = 2$ rather than the $n = 1$ compounds, with our first examples being the noncentrosymmetric DJ phases $RbBi_2Ti_2NbO_{10}$ and $CsBi_2Ti_2TaO_{10}$ (76). Both of these compounds are piezoelectric, with the compound $RbBi_2Ti_2NbO_{10}$ displaying a larger coefficient of 170 pm V^{-1} [the best-performing

$BaTiO_3$-derived variants can display coefficients as high as 1,000 pm V^{-1} (77)], as well as displaying second harmonic generation with approximately 100 times the efficiency of α-SiO_2. Notable photocatalysts are also present in the $n = 3$ phases, as shown for the DJ phase $CsBa_2Nb_3O_{10}$ (39), which according to computational results (78) is enhanced due to the inherent symmetry-breaking phenomenon. This enhanced performance is suggested as a result of the symmetry breaking of the MO_6 octahedra from the O_h point group to centrosymmetric (D_{4h}) and noncentrosymmetric (C_{4v}) point groups, where the generation of local internal fields and the promotion of electron–hole pair separation at the initial photo-oxidation step improve overall photocatalytic behavior. Similarly, $CsCa_2Ta_3O_{10}$ (79) can be nitrogen doped to be an effective visible light water oxidation catalyst (80), and nanosheets of $HCa_2Nb_2TaO_{10}$ can be utilized for photocatalytic hydrogen evolution (81). In the case of water splitting performance, the interlayer distance within RP and DJ compounds impacts how easily water can enter between the perovskite layers, which can either hinder or promote water splitting kinetics (82, 83).

Lastly, we note some interesting magnetic properties of *A*-site-ordered $n = 3$ oxides. The compounds $A[La_2Ti_3O_{10}]$ [A = Cu, Co, Zn (37), Fe (84)], one such set of compounds, were the first layered perovskites with transition metals on the *A* sites. The Fe variant in particular has been studied for its magnetic properties and was shown to be a spin glass below 30 K. It was found to have a frustration index (the ratio between the Weiss constant and the Néel temperature) of 10, indicating a highly frustrated system. Another interesting example, albeit not for magnetic applications per se, is the case of diamagnetic Ru^{2+} in the compound $Na_2La_2Ti_2RuO_{10-x}$ ($0 < x < 2$) (85), in which it was found that the Na–La–Ti–O structure was capable of stabilizing the low-spin d^6 Ru^{2+}; such stability is rare in oxide systems.

We conclude this section with a general thought on synthetic strategies for obtaining other *A*-site-ordered, as well as related, compounds. *A*-site-ordered compounds are largely prepared by conventional solid-state methods, relying on stoichiometry, difference of charge, and ionic radii to facilitate their formation. However, other methods to consider for targeting these compounds are soft chemical synthesis/intercalation methods. One interesting example is the transformations $K_2La_2Ti_3O_{10} \rightleftharpoons KLa_2Ti_3O_{9.5} \rightleftharpoons La_2Ti_3O_9$, where $La_2Ti_3O_9$ is an example of an interlayer *A*-site vacant compound (35, 43). There is also the synthetic strategy of converting materials topotactically from lower- to higher-dimensional materials, such as converting $AA'TiO_4$ compounds into higher $n = 2$ variants (86, 87).

2.1.2. *BB′* oxide layered double perovskites. There are a few examples of RP *B*-site-ordered oxides, such as the $n = 1$ $A_2Li_{0.5}B_{0.5}O_4$ [A = La; B = Co (88), Ni (88), Cu (88), Au (89)] compounds, but most form as (111) perovskites. Note that the B = Cu and Au compounds have square-planar coordination and are best described as *B*-site-ordered Nd_2CuO_4 structures. The (111) perovskite is a type of *B*-site vacant perovskite structure, well known in the halides as the layered 3-2-9 phases such as $K_3Bi_2I_9$ and $Rb_3Bi_2I_9$ (90). Most *B*-site-ordered LDP oxides present as higher-*n* versions of (111) perovskites, predominantly the 4-3-12 phase (91, 92), as well as what is described as $Ba_2Lu_{0.667}WO_6$ ($Ba_6Lu_2W_3O_{18}$) (93) and $Ba_2Gd_{0.33}ReO_6$ ($Ba_6GdRe_3O_{18}$) compounds (92), which are similar to the aforementioned 4-3-12 phase but, for charge balance, have partial *B*-site vacancies. In general, we believe that (111) perovskite structures have higher prevalence than RP/DJ phases for *B*-site-ordered compounds because the (111) structure may better stabilize the high oxidation states of the metals.

Although *B*-site ordering is the focus of this section, *A*-site compositions need mentioning, as they can dictate distortions and therefore the properties of *B*-site-ordered materials. *A*-site compositions in *B*-site-ordered oxide compounds can have just one *B*-site cation, as in $Ba_4BRe_2O_{12}$ (B = Mg, Ca, Co, Zn, Cd, In) and $Sr_4BRe_2O_{12}$ (B = Mg, Co, Ni, Zn) (94–96), or

can be mixed/ordered, as in $Ba_3LaB^{III}(W_2O_{12})$, where B = Sc, In, Lu, Yb (97). These A-site compositions can tune magnetic properties, such as in the $A_4B'B_2O_{12}$ compounds (A = Ba, Sr, La; B' = Mn, Co, Ni; B = W, Re) (96), as well as in the $A_4CoB_2O_{12}$ compounds, where different combinations of A-site cations dictate the observed ferromagnetic (FM) T_c of the system.

B-site ordering, as one might expect, also has great significance in tuning the properties of LDP oxides. In research on $Ba_3LaB^{III}(W_2O_{12})$ with B = Sc, In, Lu, Yb (98), the size of the B-site metal had a direct effect on observed superlattice signatures (tripling of the unit cell), which, on the basis of the now-known proclivity for symmetry-lowering distortions in these materials, may be another example of such behavior. Similar to the A-site ordering effect, magnetic interactions in these materials can also be tuned with B-site choice, as seen in the $Ba_2La_2NiW_2O_{12}$ ($Ba_2La_2BW_2O_{12}$) compounds (96). The interactions are antiferromagnetic (AFM) for the Mn variant and FM for the Co and Ni variants, illustrating the competition between the FM B'–O–B–O–B' and AFM B'–O–O–B' superexchange interactions. Similar effects were also seen for $Ba_2La_2NiTe_2O_{12}$ (99) and $Ba_2La_2NiW_2O_{12}$ (100), where the Te system is strongly AFM and the W system is not. The reason for this discrepancy is similar in that there are two pathways for superexchange: M^{2+}–O^{2-}–O^{2-}–M^{2+} and M^{2+}–O^{2-}–W^{6+}/Te^{6+}–O^{2-}–M^{2+}. In the W^{6+} system, these two pathways cancel out, and in the Te^{6+} system, they do not, which is a consequence of the differing electronic configurations of the two ions. Furthermore, at zero magnetic field, the Te system undergoes successive magnetic phase transitions at 9.8 and 8.9 K, indicating that the ground state spin structure is a triangular structure.

Lastly, we draw attention to the compound $Ba_3La_3Mn_2W_3O_{18}$, as B-site ordering is dependent on the thickness of the perovskite slab and may prove to be a significant component for other designer B-site-ordered LDPs (101). In this work, the authors estimated the formal oxidation state of the B sites by calculating bond valence in the structure, showing that the Mn ions are most likely in a +2 (+2.27) state and the two W atoms are in +5 (+4.89) and +6 (+6.16) states. This research showed that the W^{6+} ions are located mostly on the surface of the perovskite slab, whereas the W^{5+} ions are mainly at the central octahedral layer. This type of ordering may prove to be quite significant, especially for exfoliated materials, for which certain surface effects based on B-site ordering could be accessed.

2.2. Halide Layered Double Perovskites

The number of inorganic halide LDPs is much smaller than the number of oxides, even though the prototypic layered perovskite, K_2NiF_4, is a halide. One of the few LDP fluorides that does satisfy the definition given in Section 1 is $K_4Fe_3F_{12}$, which is an example of a layered (111) perovskite phase (102). It qualifies as an LDP by virtue of its Fe^{2+}/Fe^{3+} mixed valence behavior, whereby the Fe^{2+} and Fe^{3+} cations are on different crystallographic sites. As a consequence, $K_4Fe_3F_{12}$ is ferrimagnetic below 120 K (102) and is a Mott-Hubbard insulator (103). The Mn analog, $K_4Mn_3F_{12}$, is also known, albeit with a slightly different structure due to the need to accommodate the Jahn-Teller distortion of the Mn^{3+} ions (104). It therefore exhibits both charge and orbital ordering. By contrast, the conventional RP phase, $K_3Cu_2F_7$, is also orbitally ordered (105), but it does not technically qualify as a double perovskite, because there is only one Cu^{2+} on the B sites (106). We also note a few examples of layered (111) perovskite phases in which the A-site cations are ordered, e.g., $Ba_2RbFe_2F_9$ (107).

There is growing interest in LDP chlorides, bromides, and iodides due to their structural similarity to the inorganic and hybrid lead halide perovskites, such as $CsPbX_3$ and $(MA)PbX_3$ (X = Cl, Br, I), which are renowned for their outstanding optoelectronic properties (9). Although quite a few examples of hybrid LDP chlorides have been reported, as discussed in Section 3, practical examples of inorganic systems are few. One important exception is $Cs_4CuSb_2Cl_2$, which is a mixed

metal (111)-oriented layered perovskite that incorporates Cu^{2+} and Sb^{3+} into *B*-site layers that are three octahedra thick (i.e., $n = 3$) (23). $Cs_4CuSb_2Cl_{12}$ is a direct-band-gap semiconductor with a band gap of 1.0 eV, which is lower than that of the well-known (MA)PbI_3. It is of significant interest in relation to the quest for nontoxic relatives of the (MA)PbX_3 family. There is also a report of $Cs_4AgBiBr_8$ and $Cs_3AgBiBr_7$, which a recent article on hybrid LDPs referred to in passing, but details of their properties are outstanding (27).

An example closely related to the $Cs_4BB'_2X_{12}$ family is the series $Cs_4Mn_{1-x}Cu_xSb_2Cl_{12}$ ($x = 0$ to 1), which is again of the (111) layered perovskite type (108). In this case, the band gap can be tuned between 1.0 and 3.0 eV by varying x. The $x = 0.0$ and $x = 1.0$ end members, $Cs_4MnSb_2Cl_{12}$ and $Cs_4CuSb_2Cl_{12}$, exhibit AFM and Pauli paramagnetic behavior due to their insulating and conducting properties, respectively.

In spite of limited success in the laboratory to date, there has been recent density functional theory (DFT) theoretical work on the $Cs_4BB'_2X_{12}$ family. For example, a recent study explored the optoelectronic potential of the $A_{n+1}B_nX_{3n+3}$ layered perovskites, focusing on the family with compositions $Cs_{3+n}B^{II}{}_nSb_2I_{9+3n}$ (B^{II} = Sn, Ge), where n is the number of *B*(II) layers (109). Relative to the normal two-layer compound ($Cs_3Sb_2I_9$), improved band gaps, smaller effective carrier masses, larger dielectric constants, lower exciton binding energies, and higher optical absorption were predicted when SnI_6 or GeI_6 octahedral layers were inserted between the Sb_2I_9 bilayers in the 2D material. Adjusting the thickness of the inserted octahedral layers enabled tuning of the band gaps and effective carrier masses over a large range. Another recent theoretical study described a search for novel transparent conductors rather than new optoelectronic materials (110). In a survey of 54 potential compositions ($B^{2+} = Mg^{2+}$, Ca^{2+}, Sr^{2+}, Zn^{2+}, Cd^{2+}, Sn^{2+}; $B'^{3+} = Sb^{3+}$, In^{3+}, Bi^{3+}; $X = Cl^-$, Br^-, I^-), seven compounds were predicted to have ideal properties for *p*-type transparent conductors, with $Cs_4CdSb_2Cl_{12}$ showing particular promise. There continues to be computational work in this area (111), but there is clearly an opportunity for more progress on the experimental side.

This section on halides would not be complete without reference to an interesting variation on the theme in which the doubling of the LDP arises due to the ordering of two different halide anions (112). $Cs_2PbI_2Cl_2$ is a classical RP layered perovskite of the K_2NiF_4 type, but with the unusual feature that the I^- and Cl^- anions are fully ordered; the I^- ions are in the axial positions and the Cl^- ions are in the equatorial sites of the BX_6 octahedra. Both DFT calculations and experimental studies indicate that other mixed anion compositions of $Cs_2PbX_2Y_2$ (X/Y = Cl, Br, I) are unstable with respect to disproportionation into alternative products. In addition to having interesting optoelectronic properties as an anisotropic wide-band-gap material, $Cs_2PbI_2Cl_2$ shows promise as a high-density material for α-particle detection. The analogous tin compounds, $A_2SnI_2Cl_2$ (A = Rb, Cs), have also been reported (113), and there has been recent theoretical work on the optoelectronic properties of $Cs_2PbI_2Cl_2$ and $Cs_2SnI_2Cl_2$ (114).

Finally, we note other variations on the same theme, including the preparation of $Cs_3Bi_2I_6Cl_3$, which adopts the (111) layered perovskite structure of $Cs_3Sb_2I_9$, with Cl^- in the bridging sites and I^- in the terminal sites (115, 116). Interestingly, the parent compound, $Cs_3Bi_2I_9$, adopts a structure containing the $Bi_2I_9^{3-}$ dimer rather than the layered $Cs_3Sb_2I_9^-$-type structure. The bromide analog, $Cs_3Bi_2I_6Br_3$, exhibits very similar behavior (117).

2.3. Mixed Anion Layered Double Perovskites

Mixed anion systems are numerous and diverse (118, 119) and can display interesting properties similar to those of their monoanion parents. However, the second anion, with its potentially different charge, covalency, size, and coordination, offers a simple way to tune properties that are

relevant to applications. As in above sections, we discuss select examples in which the ions are ordered, and we provide insight into how to make mixed anion LDPs or how to characterize a compound to see whether it has anion ordering. For example, when designing a new material, a researcher can utilize Pauling's second rule as a design guide, as discussed by Fuertes (120). The rule states, "In a stable coordination structure the electric charge of each anion tends to compensate the strength of the electrostatic valence bonds reaching to it from the cations at the centers of the polyhedra of which it forms a corner" (120). If the known structural type (LDP in this case) and available sites/coordination numbers for the anions and cations are known, one can deduce the likelihood of ordering of specific anions. If the compound has already been made and ordering is yet to be established, we discuss methods below, particularly in Section 2.3.1, for issues to be considered.

We also note here that many mixed anion phases are on the edge of qualifying as LDPs. Although such mixed anion phases have sufficient ordering to qualify as LDPs, they cannot be considered LDPs because some of the observed *B–X* bond lengths are consistently long. For example, for many oxychlorides, the metal–chloride bond lengths are often more than 3 Å, which is much longer than the expected lower bound for a covalent bond length of 2.4 Å. Other researchers who have studied these compounds have taken contrasting views on how to view the *B–X* bonding; some have rationalized the compounds to be LDPs with severely distorted metal–O/*X* octahedra (55, 121), while others have regarded them as BO_5 square pyramids with counter *X* anions (122–124). Specific to the oxyhalide field, previous research did not always take advantage of DFT calculations to support the structural characterization, but one recent work on a set of new scandium oxychlorides found that the metal halide association is essentially nonbonding, and the *B* cation environment is best described as square pyramidal (125). There are, however, examples such as $CsCaNb_2O_6F$ (126), in which the *B*-site metal-fluoride interaction is clearly bonding (bond length of 2.34 Å). In general, though, a defining feature of these anion-ordered LDP structure types appears to be that they are strangely effective at inducing square pyramidal geometry in metals, even for those that are not known to commonly do so (Sc and In, in particular).

2.3.1. Oxyfluoride layered double perovskites. As oxygen and fluorine are quite similar in size, the vast majority of oxyfluoride LDPs are generally disordered (127, 128). However, a few examples are ordered, with properties similar to those of their related oxide parents. The materials can be photocatalytic (129), ionically conductive (130), magnetically significant (122, 131), and electronically conductive (132). The observed compounds have *n* values of 1 or 2, including $n = 1$ compounds like $A_2(BO_3F)$ [A = Ba, Sr; B = In (133–135) and Fe (136–138)] and $n = 2$ examples such as $RbLaNb_2O_6F$ (132). We were unable to find any $n > 2$ oxyfluorides that fit our criteria, but as there is a known chloride variant, $Sr_4Mn_3O_{8-y}Cl$ (123), we believe that a fluoride version is possible.

Ionic size is not the only thing that O and F have in common. Unfortunately, they also have near-identical X-ray and neutron scattering cross sections, and thus establishing potential anion order by X-ray or neutron diffraction is difficult. For this reason, a local probe such as NMR is commonly used to probe O/F ordering, often in conjunction with bond valence sum (BVS) calculations. As a reminder, the BVS rule states that the formal charge of a cation (anion) must be equal to the sum of the bond valences around this cation (anion). Although not always definitive and certainly not unique to the study of LDPs (130, 132), these tactics have been employed with some success for oxyfluoride LDPs. For example, in a study of $KSrNb_2O_6F$, Kim and coworkers (139) concluded that F ions likely fully occupy the innermost anion site within the perovskite slabs. In a more recent paper (126), the same authors compared $CsSrNb_2O_6F$ and $CsCaNb_2O_6F$ with similar methods and again found that the F ions likely occupy the innermost position within

the slabs. Ordering was also supported by the tendency of the Nb atoms to off-center toward the outside of the layers. This is not to say that all $n = 2$ oxyfluorides order similarly, but these examples illustrate the ways to make rational arguments, one way or another.

As a note on materials design, for the same $CsSrNb_2O_6F$ and $CsCaNb_2O_6F$ compounds (126), Kim and coauthors draw comparisons between the layered perovskites and the closely related $CsNb_2O_6F$ pyrochlore structure (140). An important takeaway is that tuning of these materials is limited, as the pyrochlore structure is a stable option for these oxyfluoride stoichiometries, and LDPs form only when the *A*-site cations are large enough (141).

2.3.2. O/Cl, O/Br, and O/I layered double perovskites. Unlike the O/F systems, the other LDP oxyhalides do not lack scattering contrast, so diffraction is an excellent way of deducing order. Furthermore, due to the differences in size and charge between O and Cl/Br/I, the likelihood of site ordering is also greatly increased in subsequent O–Cl/Br/I compounds. Oxychloride LDPs include $n = 1$ variants like A_2BO_3Cl [where A = Ca, Sr; B = Fe (142), Mn (143), Ni (122), Co (121)] and $A_2CuO_2Cl_2$ (A = Ca, Sr) (55, 144, 145); $n = 2$ examples such as $Sr_3Sc_2O_5Cl_2$ and $Ba_3Sc_2O_5Cl_2$; and an $n = 3$ compound, $Sr_8Co_6O_{15}Cl_4$ (146).

As stated in the introduction to Section 2.3, many of these Cl/Br/I compounds are close to qualifying as LDPs but are just outside our criteria and so are only briefly mentioned. In particular, the $n = 1$ $Sr_2CuO_2Cl_2$ compound is an AFM material (147) but can easily be made into a high-temperature superconductor with slight Na doping. There are also examples of Br compounds, such as Sr_2FeO_3Br (138) and $Sr_2CoO_2Br_2$ (148), and I compounds of similar structure, such as $Sr_2CuO_2I_2$ (149), as well as $n = 2$ and $n = 3$ compounds, but as the halides do not actively participate in any electronic coupling (due to their axial positions), many properties of the Br/I compounds are quite similar to those of their Cl counterparts.

2.3.3. Oxysulfide and related layered double perovskites. Oxysulfide LDPs (or even just layered perovskite sulfides) are quite rare. This is because the *B*-site metals (commonly midtransition elements) when paired with sulfur often have a proclivity to stabilize with lower oxidation states and favor tetrahedral rather than octahedral coordination. However, there are a few examples, with the expected caveat of long *B*-site metal–S bonds. These examples include $Tb_2Ti_2O_5S_2$ (150), $Sm_2Ti_2S_2O_{4.9}$ (151), $Ln_2Ti_2S_2O_5$ (Ln = Nd, Pr, Sm) (152), and $KY_2Ti_2O_5S_2$ (153). One material of note, $Y_2Ti_2O_5S_2$, is an effective photocatalyst capable of stoichiometric water splitting following spatially separated loadings of IrO_2 and Cr_2O_3/Rh as the oxygen and hydrogen evolving complexes, respectively (154).

2.3.4. O/N and related layered double perovskites. Metal oxynitrides, not just specifically LDPs, are an emerging class of materials with captivating photocatalytic and electronic properties (155–158). Their success as photocatalysts, for example, comes in part from having redshifted absorption edges relative to their oxide counterparts, which increases visible light absorption and leads to improved photocatalytic efficiency. There are a few examples of oxynitride LDPs, including the $n = 1$ RP tantalate compounds Ba_2TaO_3N (26) and Sr_2TaO_3N (159) and related niobates, such as Sr_2NbO_3N (160). Rosseinsky and coworkers (26) demonstrated that if Ba_2TaO_3N is made conventionally, the O and N atoms will be disordered, but if the N source is made with a mineralizer present, the anions will be ordered. Specifically, the equatorial anion sites within the $n = 1$ perovskite layer are predominantly populated by N, and the apical sites are occupied by O. This ordering is also achievable for Sr_2TaO_3N (161–163). These oxynitride phases exhibit high bulk dieletric constants, as do other related compounds with the general formula ABO_2N (A = Ba, Sr,

Ca; B = Ta, Nb), as shown by Tai and coworkers (164). Other interesting phases include a recent example like the compound $Eu^{II}Eu^{III}{}_2Ta_2N_4O_3$, which was made through high-temperature and high-pressure autoclave synthesis (165). This material has a small (assumed to be direct) band gap of 0.6 eV but has yet to be studied in great detail in terms of its potential optoelectronic or other properties. As a final underexplored example, there is the known compound Nd_2AlO_3N (166). No properties were reported for the material, but it is known to crystallize in the polar space group *I4/mm* (109) and may therefore warrant further exploration.

2.3.5. O/OH layered double perovskites. Much like the oxyhalides and oxysulfides, LDP oxyhydroxides can display long *B*-site metal–OH bonds. Numerous LDP oxyhydroxides appear to have been inspired by the topotactic conversion of the iron-based layered oxide $Sr_3NdFe_3O_{8.5+\delta}$ into the hydrated oxyhydroxide $Sr_3NdFe_3O_{7.5}(OH)_2{\cdot}H_2O$, and these oxyhydroxides have been studied for their magnetic properties (167–169). In the case of $Sr_3NdFe_3O_{7.5}(OH)_2{\cdot}H_2O$, the hydroxide compound forms upon exposing the oxide parent, $Sr_3NdFe_3O_{9-\delta}$, to humid air over multiple days, and the hydroxide ions order at the apical sites of the perovskite layer. This procedure is essentially the same for all other hydroxides that form topotactically from oxide parents. Maignan and coworkers (170) demonstrated that the perovskite layer thickness (and concomitant strength of magnetic interactions) in the oxide/oxyhydroxide Sr-Co-Ti-O system [the example being $Sr_3Co_{1.7}Ti_{0.3}O_5(OH)_2xH_2O$] is controlled by the Ti/Co ratio. A later article from some of the same authors (171) showed just how impactful the topotactic conversion could be for magnetic properties. For example, the oxyhydroxide $Sr_{3-\delta}Co_{1.9}Nb_{0.1}O_{4.86-\delta}(OH)_{3.04}{\cdot}0.4H_2O$ was found to be a weak ferromagnet with a $T_c \approx 200$ K, even though its parent oxide was a spin glass material with a $T_g \approx 50$ K (171).

2.3.6. O/H layered double perovskites. The oxyhydrides are an incredibly interesting class of LDPs, with both magnetic and ion conducting functionalities (172). We start with the notable example of $LaSrCoO_3H_{0.7}$ reported by Hayward (173), which was prepared by the reaction between $LaSrCoO_4$ and CaH_2. This compound is quite remarkable in that it has magnetic long-range order above room temperature, a result of the capacity of the hydride anions to strongly couple transition metal cations electronically. The hydrides present a clear distinction in this respect to other $n = 1$ ordered anion phases (except the nitrides and a few fluorides), as the hydride ion orders equatorially in the *B*-site perovskite layer, whereas the majority of other anions prefer to order at apical sites (and far away from the metal, as we have seen). This proclivity for apical ordering ultimately eliminates most anions from participating in magnetic coupling between the perovskite layers, making the hydrides an attractive class of materials for tuning electromagnetic properties. There are, however, instances in which, if the hydride ions are low enough in concentration (and therefore the compounds are not necessarily LDPs anymore), then the hydride site preference depends on the *n* value (174).

Although examples of LDP oxyhydrides were first synthesized three decades ago (175), some have recently also shown promise as high-performance ionic conductors (30, 176). Interestingly, for the LDP oxyhydride Ln_2LiHO_3, hydride ion conduction pathways were unlike the related oxide-conducting counterparts, such as La_2NiO_4 (177). The reason for the difference is thought to be that the increased covalent character of the La-O layer of the oxyhydride creates barrier channels of electron density in the structure, ultimately making in-plane migration the more favorable energy pathway for hydride migration. For oxide anions in La_2NiO_4 and other similar oxides, the ions move via an interlayer path. As the interlayer path should be more efficient due to decreased covalent bonding between Mg and O, materials like $Ba_2MgH_2O_2$ and $Sr_2MgH_2O_2$ have been proposed as better hydride ion conductors.

2.3.7. Other mixed anion layered double perovskites. Other examples of LDP compounds fall just outside of the descriptions we provide above. Some of these include combinations of halides and polyatomic anions, such as $Cs_2PbI_2(SCN)_2$ (178). This compound and its hybrid cousins (179, 180) have been studied as possible alternatives (due to their stability) to the 3D connected hybrid halide perovskites. There are also examples of LDP nitride-fluorides, like the first reported, $Ce_2MnN_3F_{2-\delta}$ (181). The preparation of this compound is quite interesting, as it was made by low-temperature fluorination of the ternary nitride Ce_2MnN_3. A combination of neutron diffraction and magnetic susceptibility studies showed mixed valence Mn and fluoride ion interstitials within a K_2NiF_4-type structure.

3. HYBRID LAYERED DOUBLE PEROVSKITES

Hybrid LDPs are LDPs that contain organic species on at least one of the *A*, *B*, or *X* sites. As *B* sites are populated almost exclusively with metal cations, the *A* and *X* sites provide the most variation for organic substitution. Hybrid LDPs can be further characterized into four main categories: *AA′* type I, *AA′* type II, *BB′*, and *XX′*, as illustrated in **Figure 3**, which displays the relevant schemes.

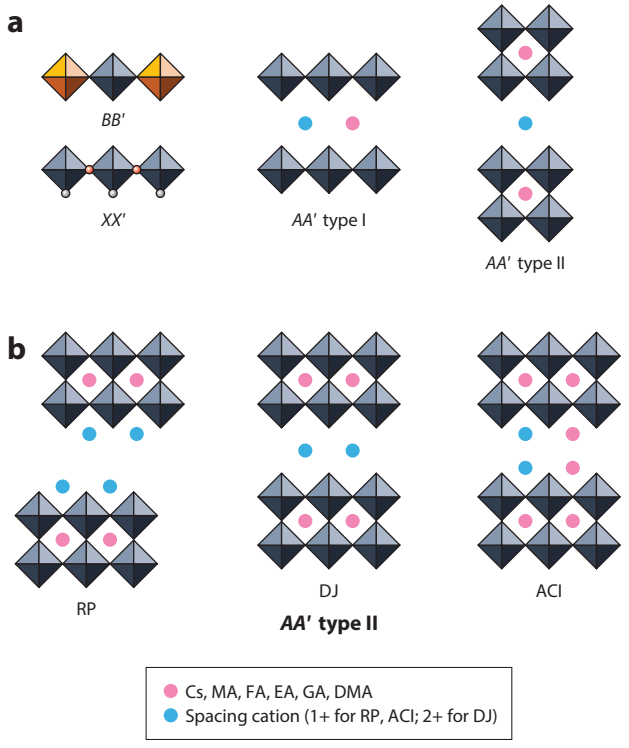

Figure 3

(*a*) Schematic illustration of different types of hybrid layered double perovskites: *BB′* involving ordering on the metal *B* site, *XX′* involving ordering on the linkers, and two kinds of *AA′*: type I, with cations ordering between layers, and type II, with cations ordering within and outside cages. (*b*) Schematic illustration of *AA′* type II structures, RP, DJ, and ACI. Abbreviations: ACI, alternating cations in the interlayer space; DJ, Dion-Jacobson; DMA, dimethylammonium; EA, ethylammonium; FA, formamidinium; GA, guanidinium; MA, methylammonium; RP, Ruddlesden-Popper.

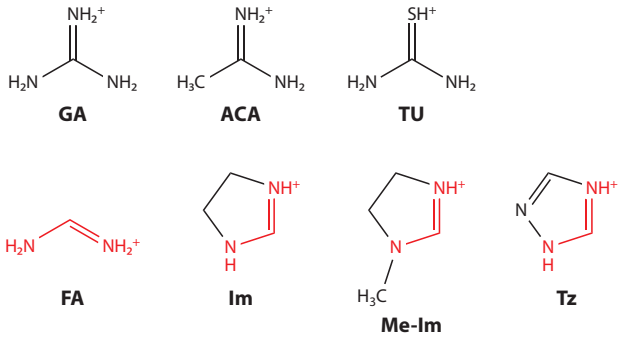

Figure 4

Some of the amine cations that are commonly employed in the stabilization of layered hybrid halide perovskite compounds, including hybrid layered double perovskites (182–189). Similar functional group identities are highlighted in red. Abbreviations: ACA, acetaminidium; FA, formamidinium; GA, guanidinium; Im, imidazolium; Me-Im, methylimidazolium; TU, protonated thiourea; Tz, 1,2,4-triazolium.

Figure 4 depicts the different amine cations that are frequently found to assist in the formation of LDPs. As we do above for the subsections within Section 2, here we select representative cases from each category and assess areas of possible expansion for new materials.

3.1. *AA′* Hybrid Layered Double Perovskite Halides

This section discusses *A*-site-ordered hybrid compounds.

3.1.1. *AA′* type I hybrid layered double perovskites. *AA′*-type ordering is unique to hybrid LDPs and is characterized by having both *A* and *A′* cations ordered within the same interlayer space ($n = 1$ LDP only). As a general note, if the compounds have the same perovskite layer orientation/composition, the materials will usually have similar properties, regardless of the *A*-site cations of choice. However, as many organic cations have variable size and functionality, changing between organic cations can inadvertently template new perovskite layer orientations and can therefore change properties. This templating effect is a defining feature of the *AA′* type I compounds and gives rise to the cation-ordered (100)-, (110)-, and (210)-oriented structures seen in **Figure 5**. With more perovskite layer orientations (in addition to the RP and DJ phases seen in Section 2), hybrid LDPs display a great degree of structural and synthetic variability. For instance, some researchers reported combining GA and smaller cations (Cs or MA) to obtain (100)-oriented structures like (GA)$CsSnBr_4$ and (GA)(MA)PbI_4 (182, 183), while others have reported that by using a larger *A′* cation such as imidazolium (Im), methylimidazolium (Me-Im), or 1,2,4-triazolium (Tz), (110)-oriented structures like (GA)(Im)$PbBr_4$ and $(GA)_{1.5}(Me\text{-}Im)_{0.5}SnI_4$ can be made (184, 185). There are also examples with mixed *A*-site cations, such as $(GA)_{1.5}(Me\text{-}Im)_{0.5}SnI_4$, in which the stoichiometry is nontypical, as GA cations share the same cavities with Me-Im cations. To our knowledge, there are no inorganic LDP examples similar to $(GA)_{1.5}(Me\text{-}Im)_{0.5}SnI_4$. There are also instances of (110)-oriented structures, including (HEA)(FA)$PbBr_4$ (HEA = hydroxyethylammonium; FA = formamidinium), reported by Salah et al. (186). Guo et al. (187) recently reported a 3 × 3–type (110)-oriented compound, (Im)(Tz)$PbBr_4$. In 2018, Nazarenko et al. (188) and Daub & Hillebrecht (189) first demonstrated the (210)-oriented type, which is the least common of the possible perovskite orientations. Both groups reported the structure of (GA)(FA)PbI_4, but Daub & Hillebrecht (189) also reported (Tu)(FA)PbI_4 (Tu = protonated thiourea), which formed with

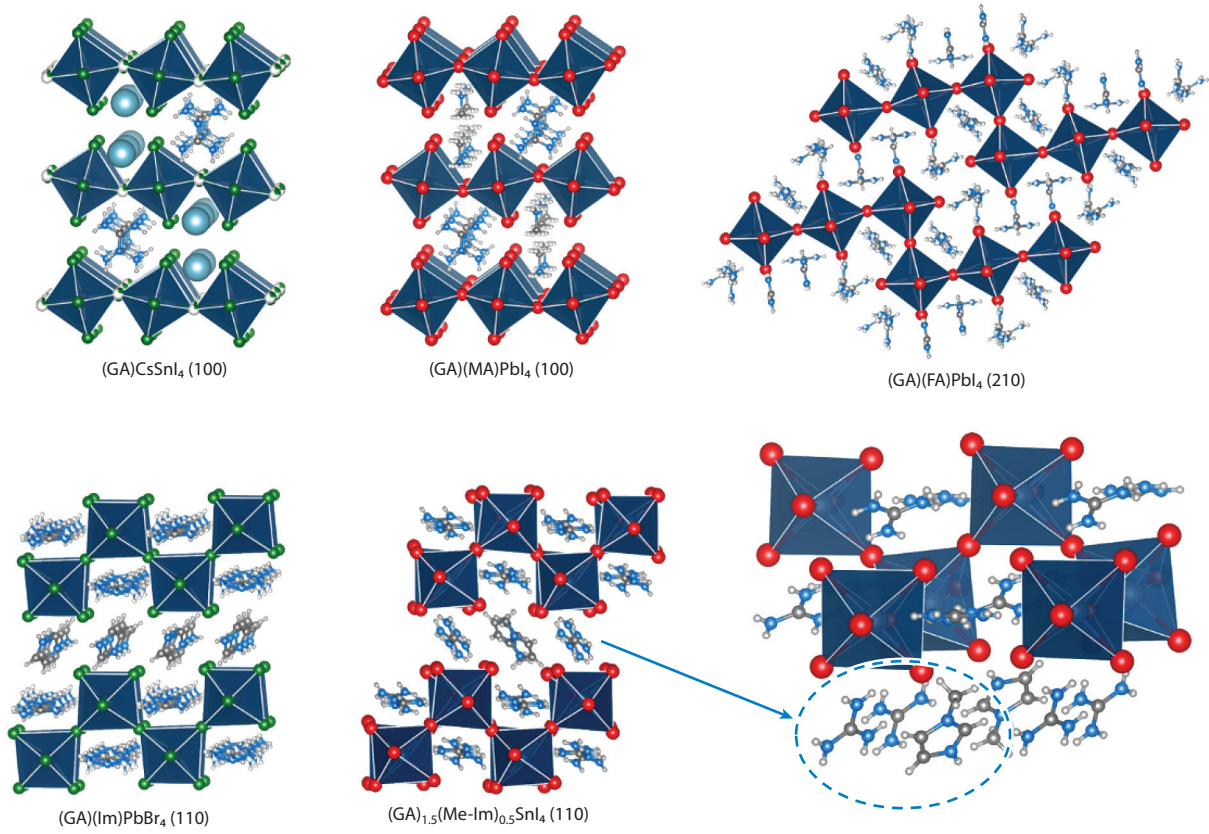

Figure 5

Example structures with different types of either (100) (182, 183), (210) (188, 189), or (110) (184, 185) layer orientations. Abbreviations: FA, formamidinium; GA, guanidinium; Im, imidazolium; MA, methylammonium; Me-Im, methylimidazolium.

the same (210)-oriented structure. This result is not too surprising, given that GA and Tu are similar in shape, size, and functionality and would be expected to have similar templating effects (see **Figure 4**).

From these observations, we can generalize a structural trend: GA/Tu/ACA (acetamidinium) plus a small cation like Cs or MA will create a (100)-oriented compound; GA/Tu/ACA plus a larger cation (with similar functional group identity shown in **Figure 4**) will create either (210)- or (110)-oriented-type LDPs. Thus, there are plenty of opportunities to create new structures by using the less explored Tu and ACA cations, but also note that stoichiometry plays a vital role in designing these hybrid compounds. For example, when the ratio of AA' cations changes from either 2:1 or 1:1 to 1:2, the structures can be distinct, with potentially more than one cation occupying multiple sites within the structure.

3.1.2. AA' type II. The AA' type II double perovskite is defined by A cations occupying the perovskite cages and the A' cations (as well as A cations in some cases) ordering between the perovskite layers. Phase AA' type II is similar to AA' type I, where both A' and A cations are found in interlayer sites, but also with A cations in the perovskite cages. In most cases of RP, DJ, and ACI (alternating cations in the interlayer space) structures, the A cations and A' spacing

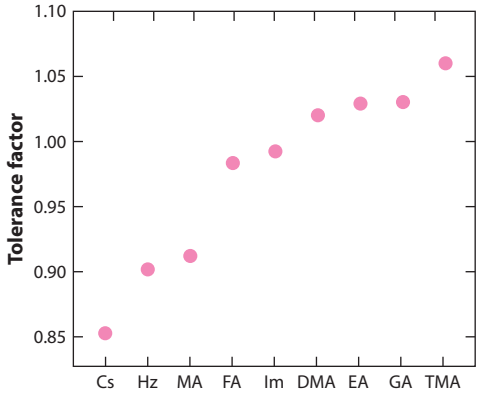

Figure 6

The perovskite tolerance factor of the smaller *A* cations employed in the preparation of hybrid layered double perovskites. Abbreviations: DMA, dimethylammonium; EA, ethylammonium; FA, formamidinium; GA, guanidinium; Hz, hydrazinium; Im, imidazolium; MA, methylammonium; TMA, trimethylammonium. Adapted from Reference 195.

cations are different species, so the way they form qualifies as naturally *AA′* type II, as shown in **Figure 3**, except for $(EA)_4Pb_3Cl_{10}$, $(EA)_4Pb_3Br_{10}$, and $(IPA)_3Sn_2I_7$ (EA = ethylammonium, IPA = isopropylammonium). Extensive examples of layered perovskite RP, DJ, and ACI phases have been discussed in other reviews (190–192).

With regard to *A*-site cation choice, a particularly recent and interesting discovery in 2D halide perovskites is that *A* cations (within the perovskite cages) are not limited to MA, FA, or Cs, unlike for 3D perovskites. Fu and coauthors (193, 194) first reported a series of $n = 2$ compounds, $(HA)_2APb_2I_7$, where HA is *n*-hexylammonium and *A* = MA, FA, DMA, EA, GA, and ACA. Among these compounds, the examples in which *A* = DMA, EA, GA, and ACA have tolerance factor ratios of above 1 (**Figure 6**) (193), which contrasts with the usual Goldschmidt tolerance factor guideline of values between 0.8 and 1.0. The more lenient tolerance factor requirement here is attributed to the flexibility of the 2D framework, as strain can be accommodated more easily by the 2D RP structures. Additionally, $n = 3$ structures have been made, such as $(BA)_2(EA)_2Pb_3I_{10}$ (196, 197), where the EA-based structure displays blueshifted absorption and photoluminescence due to the larger distortion in the inorganic framework. Li et al. (198) subsequently expanded upon this work and reported the $(BA)_2APb_2I_7$ series (*A* = MA, FA, DMA, and GA), showing that this rule also applies when the spacing cation is changed to BA.

3.2. *BB′* Hybrid Layered Double Perovskite Halides

A defining feature for LDPs and hybrid LDPs especially is that, for certain *B*- or *X*-site compositions for which a 3D perovskite phase is unstable, a 2D analog may still form. For example, the iodide-based double perovskite Cs_2AgBiI_6 has not been synthesized, because it has an unfavorable tolerance factor value and because it is competing against the favorable formation of $Cs_3Bi_2I_9$. However, several iodide hybrid LDPs have been made. These phases include, for example, $(AE2T)_2AgBiI_8$, $(CHDA)_2AgBiI_8$, $(AMP)_4AgBiI_8$, and $(IPA)_4AgBiI_8$ (where AE2T = 5,5-diylbis(amino-ethyl)-[2,20-bithiophene], CHDA = 1,4-cyclohexanediammonium, AMP = 4-aminomethylpiperidinium, I-PA = 3-iodopropylammmonium) (see **Table 1**). The first case of an iodide-based hybrid LDP was $(AE2T)_2AgBiI_8$, reported by Jana et al. (199); the dication AE2T was employed. Bi et al. (200, 201) subsequently reported a series of I-based hybrid LDPs, with

Table 1 Summary of optical and electronic properties of 2D hybrid double perovskites reported to date

Compound	E_g (eV)	Electronic structure
Cl based		
$(PA)_4AgInCl_8$ (202)	3.96	Indirect
$(BA)_4AgInCl_8$ (203)	4.27	N/A
$(BA)_4CuInCl_8$ (203)	3.47	N/A
$(BA)_4AgSbCl_8$ (203)	3.22	N/A
Br based		
$(BA)_4AgBiBr_8$ (27)	2.60	Direct
$(PA)_4AgBiBr_8$ (202)	2.41	Inconclusive
$(OCA)_4AgBiBr_8$ (202)	2.45	N/A
$(BDA)_2AgBiBr_8$ (202)	2.43	Inconclusive
$(Cl\text{-}PA)_4AgBiBr_8$ (204)	2.57	Indirect
$(PA)_4AgInBr_8$ (202)	3.15	Indirect
$(BA)_4AgSbBr_8$ (203)	2.80	N/A
$(3\text{-}BPA)_4Ag\mathit{B}Br_8$; B = In, Tl (205)	≈3.25, 2.25	Indirect
$(BA)_2CsAgTlBr_7$ (205)	≈2.1	Direct
$(PEA)_2CsAgTlBr_7$ (205)	≈1.9	Direct
$(BA)_2CsAgBiBr_7$ (27, 206)	2.38	Indirect
$(PA)_2CsAgBiBr_7$ (202, 207)	2.32	Inconclusive
I based		
$[NH_3(CH_2)_8NH_3]_2$ $[(AuI_2)(AuI_5)(I_3)_2]$ (208)	1.14	N/A
$(AE2T)_2AgBiI_8$ (199)	2.0	Direct
$(CHDA)_2\mathit{B}BiI_8$; B = Ag, Cu (200)	1.93, 1.68	Indirect
$(CAA)_nCuBiI_8$ (n = 2 or 4) (201)	1.5–1.6	Direct
$(I\text{-}PA)_4AgBiI_8$ (209)	1.87	Indirect
$(AMP)_4AgBiI_8$ (210)	2.0	Direct
$(APP)_4AgBiI_8$ (210)	2.05	Direct

Abbreviations: 3-BPA, 3-bromopropylammonium; AE2T, 5,5-diylbis(amino-ethyl)-[2,20-bithiophene]; AMP, 4-aminomethylpiperidinium; APP, 4-aminopiperidinium; BA, butylammonium; BDA, butyldiammonium; CAA, cyclo-octylammonium; CHDA, 1,4-cyclohexanediammonium; I-PA, 3-iodopropylammmonium; N/A, not applicable; OCA, octylammonium; PA, propylammonium; PEA, phenethylammonium.

the B site being either Cu or Ag, the B' site being Bi, and the A site spanning a series of mono- and dications. This increased stability window, especially in the case of the iodides, is related to the aforementioned capacity to bypass the tolerance factor limitations of the A site. The recent development of hybrid LDP halides was catalyzed by a report from Connor et al. (27), who demonstrated dimensionality reduction of the 3D double perovskite $Cs_2AgBiBr_6$ by incorporating BA into the synthesis; this resulted in the formation of $(BA)_4AgBiBr_8$ (single layered, n = 1) and $(BA)_2CsAgBiBr_7$ (double layered, n = 2) (27).

In addition to the more predictable phases derived from 3D double perovskites, such as $(BA)_4AgBiBr_8$ (parent: $Cs_2AgBiBr_6$) and $(PA)_4AgInCl_8$ (PA = propylammonium; parent: $Cs_2AgInCl_6$), unexpected phases like $(PA)_4AgInBr_8$ (the parent compound $Cs_2AgInBr_6$ has not been reported) have been demonstrated. More new phases are expected to be made, either by adding different organic spacer cations to existing 3D systems, such as the compounds listed in

Table 1, or by using different octahedrally coordinated B (1+) and B' (3+) cations, as shown in **Figure 5**. Typical 1+ metal cations that can adopt octahedral geometry include the alkali metals Na and K (Li is usually too small, and Rb and Cs too large) and the coinage metals Cu, Ag, and Au. Metals that can be 3+ with octahedral coordination include Sc, Y, Ti, V, Cr, Mo, Fe, Ru, Co, Au, lanthanides, actinides, and group III elements.

Although the organic layer can impact properties by templating the perovskite layer, the optical and electronic properties of the BB'-type hybrid LDPs are more dependent on the metal and halide composition. In a system in which only the thickness of the layer varies, such as $(BA)_4AgBiBr_8$ ($n = 1$) and $(BA)_2CsAgBiBr_7$ ($n = 2$), the band gaps (absorption edge) of the $n = 1, 2$ compounds, and the 3D parent $Cs_2AgBiBr_6$, are ≈2.6, ≈2.4, and ≈2.2 eV, respectively (27). Relative to a Pb-based system like $(BA)_2(MA)_{n-1}Pb_nBr_{3n+1}$, the jump between $n = 1$ and 3D has a much more significant effect on the optical properties. The band gap decreases from ≈3.0 eV ($n = 1$) to ≈ 2.25 eV [3D $(MA)PbBr_3$] (211). As such, there has been a drive to increase the layer thickness of both hybrid LDPs as much as possible. Doing so, however, is difficult, and there have not been any reports of new B-site-ordered hybrid LDPs with $n > 2$.

For B-site-ordered materials, the role of the organic cation is often marginal. In a previous report (202), $A_nAgBiBr_8$ ($n = 2$ or 4) materials based on the organic A cations PA, BA, octylammonium (OCA), and butyldiammonium (BDA) had similar band gaps in the range of 2.41 to 2.45 eV. Woodward and coworkers (203) also reported four hybrids with BA as the spacing cation; they used solid-state synthesis to make $(BA)_4CuInCl_8$, $(BA)_4AgInCl_8$, $(BA)_4AgSbCl_8$, and $(BA)_4AgSbBr_8$. Likewise, Bi et al. (201) reported a series of A_nCuBiI_8 ($n = 2$ or 4) materials with different organic cations, where the band gap of the materials spans a narrow range between 1.55 and 1.65 eV. An interesting discovery from both reports is that materials with larger interlayer distances generally have slightly larger band gaps. Another characteristic observed by Bi et al. (201) is that the band gap increases with smaller Cu–I–Bi angles, making this situation similar to Pb- or Sn-based 2D systems, in which larger B–X–B' angles correspond to smaller band gaps. However, of the two structures reported, the Cu atom is split (disordered) on average, making the Cu–I–Bi angles from two of the structures difficult to quantify on a local scale. Nevertheless, in this instance, the organic cations have some impact on the overall structure and properties of hybrid LDP systems. The direct and indirect effects need to be evaluated on a case-by-case basis, but between templating or changing interlayer space, their role can be sometimes benign and sometimes impactful.

That said, a wide range of property tunability is possible for B-site-ordered hybrid LDPs, with band gaps spanning a remarkable 2.3 eV (≈1.7 to ≈4 eV), depending on the choice of halide. The band gaps are smallest and largest for iodide and chloride materials, respectively. However, finer tuning of optical properties is possible by changing B-site metal composition, as demonstrated with $(CHDA)_2CuBiI_8$ (≈1.68 eV) and $(CHDA)_2AgBiI_8$ (≈1.93 eV) (201). Thus, by changing the B-site cation (1+) from Cu to Ag, one can enlarge the band gap. This behavior is also demonstrated in the cases of $(BA)_4CuInCl_8$ and $(BA)_4AgInCl_8$, in which the band gap increases from ≈3.47 eV (Cu) to ≈4.27 eV (Ag) (27). In the BA-based bromide systems, the corresponding B' cation varies from In to Sb to Bi; these compounds show a band gap trend of In > Sb > Bi, where $(BA)_4AgInBr_8$, $(BA)_4AgSbBr_8$, and $(BA)_4AgBiBr_8$ have band gaps of ≈3.32, ≈2.80, and ≈2.65 eV, respectively (27, 203).

Particularly interesting cases of hybrid LDPs include the following. In 2003, Castro-Castro & Guloy (208) reported a special type of hybrid LDP, with mixed valence Au^I and Au^{III}: $[NH_3(CH_2)_8NH_3]_2[(Au^II_2)(Au^{III}I_4)(I_3)_2]$ and $[NH_3(CH_2)_7NH_3]_2[(AuAu^{III}I_2)(Au^{III}I_4)(I_3)_2]$. In these compounds, $[Au^II_6]$ octahedra are compressed tetragonally, whereas the terminal iodides in $[Au^{III}I_6]$ are composed of partial polyiodides I_3^-. The optical band gaps for these compounds are

≈1.14 and ≈0.95 eV, respectively, which are lower than that of $Cs_2Au_2I_6$ (≈1.31 eV) or presumably $(MA)_2(Au_2I_6)$ (212); this lowering of the band gap can potentially be explained by the incorporation of I_3^-. There is also the recently reported I-based hybrid, $(IPA)_4AgBiI_8$, where the spacing cation IPA was originally 3-bromopropylammmonium, which reacted in situ with hydroiodic acid to become 3-iodipropylammonium (209).

There have been several computational studies of hybrid LDPs using DFT. The calculated electronic structure of the 3D double-perovskite $Cs_2AgBiBr_6$ has an indirect band gap, where the conduction band minimums (CBMs) consist of Ag *s*, Bi *p*, and Br *p* orbitals and the valence band maximums (VBMs) consist of Ag *d*, Bi *s*, and Br *p* orbitals (206, 213). When Connor et al. (27) reported the hybrid LDP derivatives of $Cs_2AgBiBr_6$ [$n = 1$ compound $(BA)_4AgBiBr_8$ and $n = 2$ compound $(BA)_2AgBiBr_7$], calculations showed a frontier orbital composition similar to that of the 3D parent compound, but interestingly, the $n = 1$ compound had a direct band gap. Connor et al. explicitly attributed this indirect-to-direct change to dimensionality reduction. Conversely, Tran et al. (214) reported a counterexample of a direct-to-indirect change of a band gap by replacing In with Sb in $Cs_2AgSb_xIn_{1-x}Cl_6$ solid solutions. Their calculations showed that $Cs_2AgInCl_6$ had a direct band gap and that, by increasing the amount of Sb, the CBM became defined by the Sb 5*p* orbital (with a transition observed at $x = 0.4$), and the transition became indirect. Additionally, for the PA end member compound of the same *B*-site composition, $(PA)_4AgInCl_8$, calculations indicate the band gap to be indirect (202). Moreover, because of the relatively flat bands, the band gap of the related compound $(BDA)_2AgBiBr_8$ is difficult to discern as either direct or indirect (202).

Similarly, when Jana et al. (199) reported the first iodide-based hybrid layered double perovskite, $(AE2T)_2AgBiI_8$, the calculated band gap was reported to be indirect without spin-orbit coupling (SOC), but direct with SOC. More recently, Karunadasa and coworkers (205) reported that the $n = 2$ structure $(PEA)_2CsAgTlBr_7$ (PEA = phenethylammonium) has a direct band gap, where the VBM is composed of Ag *d* and Br *p* orbitals and the CBM is composed mainly of Tl *s* and Br *p* orbitals, similar to the 3D double perovskite $Cs_2AgTlBr_6$. The band gap of the $n = 1$ compound, however, was found to be indirect, originating from Ag-to-Tl metal charge transfer. A more detailed list of the reported LDPs and the nature of their electronic structures can be found in **Table 1**.

In general, relative to Pb- or Sn-based layered perovskites, hybrid LDPs generally have flatter bands. The situation is therefore not as clear as in the Pb- or Sn-based systems, in which the materials have direct band gaps. From the results regarding hybrid LDPs, we can see that the nature of the band gap is highly dependent on metal composition. Layer thickness and local structural distortion may also play a part in determining the direct-to-indirect transition. Careful theoretical work is needed before generalizing the trend on the basis of either the parent 3D material or simply the dimensionality reduction.

3.3. Hybrid Layered Double Perovskites with Polyatomic Anion Linkers

Only a few examples of hybrid LDPs with organic or polyatomic linkers on *X* sites are known. In principle, it is possible to form these layered structures with linkers such as formate, nitrate, azide, imidazolate, and cyanide, as these have been well documented to make perovskite-type structures with suitable single-metal compositions (8, 215). In contrast to the many halide examples discussed above, however, the metal and the *X*-site linkers in hybrid LDPs can display multiple types of coordination modes, often creating more complex structures. An LDP formate with Na^+ and Al^{3+} using the cation *N*, *N*′-dimethylethylenediammonium (DMEN) (**Figure 7*a***) has been reported (216). The coordination modes between the formate linkers and the

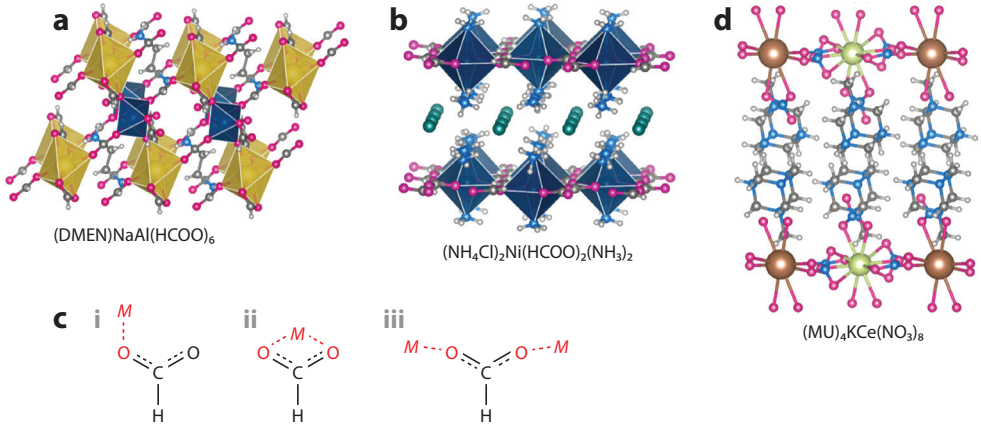

Figure 7

(*a*,*b*) Crystal structure of (*a*) (DMEN)NaAl(HCOO)$_6$ (216) and (*b*) $(NH_4Cl)_2[Ni(HCOO)_2(NH_3)_2]$ (220). (*c*) Depiction of different formate coordination modes with metals. (*d*) Crystal structure of $(MU)_4KCe(NO_3)_8$ (221). Abbreviations: DMEN, *N*, *N*-dimethylethylenediammonium; *M*, metal; MU, methylurotropinium.

metals in (DMEN)NaAl(HCOO)$_6$ are also listed, illustrating the multiple types (**Figure 7*c*,*i–iii***) present in the structure. This bonding contrasts with the bonding seen for formate perovskites or the analogous hypophosphite perovskites and ReO_3-type structures (217–219). Understandably, the possibility of several bonding modes makes designing a layered structure difficult, as the formation of a more extended and complex structure may result, depending on the metal and *A*-site cation of choice. However, multiple *X*-site anions can be included to diminish this effect. For example, in the case of the *X*-site-ordered hybrid LDP $(NH_4Cl)_2[Ni(HCOO)_2(NH_3)_2]$ (220) (**Figure 7*b***), the formate links the Ni atoms together in the equatorial positions, and ammonia caps Ni at the axial positions. In this example, only the easily understood bonding mode (**Figure 7*c*,*iii***) is present.

Another recent example used nitrate as the bridging linker (with doubling on the *B* site) to yield a series of new compounds (221). Shi et al. (221) found that by using chiral *R*/*S*-3-fluoroquinuclidinium, *R*/*S*-3-chloroquinuclidinium, and *R*/*S*-4-fluoro-1-azabicyclo[3.2.1]-octanium cations, noncentrosymmetric structures could be made. They investigated multiple B^{I} and B'^{III} combinations, such as K^+ with Ce^{3+} (**Figure 7*d***); Rb^+ with Tb^{3+}, Dy^{3+}, Eu^{3+}, and Sm^{3+}; and Cs^+ with Sm^{3+}. Interestingly, NH_4^+ can also act as a 1+ cation on the *B* site and formed an hybrid LDP structure with Ce^{3+}. The discovery of noncentrosymmetric, second-harmonic-generation active materials combined with the emissive nature of the rare earth metals opens a new pathway to engineer multifunctional hybrid materials.

4. CONCLUSION

In this review of LDPs, we lay out a case for the hitherto unrecognized richness of structure in this large family of crystalline compounds, accompanied by an equal wealth of properties, whose tuning is accomplished through the many different compositional knobs that can be turned. Below, the Summary Points capture the essence of what has been covered in the fields of inorganic and hybrid LDPs, while the Future Issues draw attention to some of the most exciting avenues for further study.

SUMMARY POINTS

1. The chemical diversity of layered double perovskites (LDPs) is much greater than has hitherto been recognized, especially with the recent emergence of hybrid LDPs in which protonated amines play the role of some, or all, *A* cations.
2. In the case of inorganic LDPs, there is now an enormous family of compounds that are doubled due to ordering of different ions on *A*, *B*, or *X* sites. Furthermore, these compounds show an extensive range of functionalities, including remarkable magnetic, electronic, spectroscopic, electrochemical, and catalytic properties.
3. The field of hybrid LDPs is less mature, but they, especially the halide LDPs, show great promise. The low dimensionality of halide LDPs facilitates the formation of important compounds, such as iodides, that do not normally form as 3D double perovskites.

FUTURE ISSUES

1. Certain areas of inorganic LDPs have been neglected to date but would be worthy of future exploration. The absence of chalcogenide LDPs is particularly striking, and study in this area could present some exciting opportunities for the future.
2. In the case of hybrid LDPs, the focus has been largely on the halides of the posttransition metals, largely due to their relationship with the important hybrid perovskites of lead. We see many opportunities in the study of hybrid LDPs based on transition metals and rare earths, in which exploring the magnetic and spectroscopic properties could be of great interest.
3. Beyond the current focus on hybrid LDP halides, there is also great scope for work on LDPs containing polyatomic anionic linkers, in much the same way that this area has become very important for the 3D perovskites. Such linkers would include formates, hypophosphites, azides, and cyanides, most of which are known to form 2D and 3D perovskites, some of them doubled.

DISCLOSURE STATEMENT

The authors are not aware of any affiliations, memberships, funding, or financial holdings that might be perceived as affecting the objectivity of this review.

ACKNOWLEDGMENTS

H.A.E. thanks the US National Research Council for financial support through the Research Associate Program. L.M. and R.S. have been supported by the US Department of Energy, Office of Science, Basic Energy Sciences, under grant SC0012541. A.K.C. acknowledges the Ras Al Khaimah Center for Advanced Materials for supporting this research.

LITERATURE CITED

1. Goldschmidt VM. 1926. Die Gesetze der Krystallochemie. *Naturwissenschaften* 14:477–85
2. Megaw HD. 1946. Crystal structure of double oxides of the perovskite type. *Proc. Phys. Soc.* 58:133

3. von Hippel A. 1950. Ferroelectricity, domain structure, and phase transitions of barium titanate. *Rev. Mod. Phys.* 22:221–37
4. Sleight AW, Gillson JL, Bierstedt PE. 1993. High-temperature superconductivity in the $BaPb_{1-x}Bi_xO_3$ system. *Solid State Commun.* 88:841–42
5. Wu MK, Ashburn JR, Torng CJ, Hor PH, Meng RL, et al. 1987. Superconductivity at 93 K in a new mixed-phase Y-Ba-Cu-O compound system at ambient pressure. *Phys. Rev. Lett.* 58:908–10
6. von Helmolt R, Wecker J, Holzapfel B, Schultz L, Samwer K. 1993. Giant negative magnetoresistance in perovskitelike $La_{2/3}Ba_{1/3}MnO_x$ ferromagnetic films. *Phys. Rev. Lett.* 71:2331–33
7. Jin S, Tiefel TH, McCormack M, Fastnacht R, Ramesh R, Chen L. 1994. Thousandfold change in resistivity in magnetoresistive La-Ca-Mn-O films. *Science* 264:413–15
8. Li W, Wang Z, Deschler F, Gao S, Friend RH, Cheetham AK. 2017. Chemically diverse and multifunctional hybrid organic–inorganic perovskites. *Nat. Rev. Mater.* 2:16099
9. Kojima A, Teshima K, Shirai Y, Miyasaka T. 2009. Organometal halide perovskites as visible-light sensitizers for photovoltaic cells. *J. Am. Chem. Soc.* 131:6050–51
10. Wang X-Y, Gan L, Zhang SW, Gao S. 2004. Perovskite-like metal formates with weak ferromagnetism and as precursors to amorphous materials. *Inorg. Chem.* 43:4615–25
11. King G, Woodward PM. 2010. Cation ordering in perovskites. *J. Mater. Chem.* 20:5785–96
12. Sarma D, Sampathkumaran E, Ray S, Nagarajan R, Majumdar S, et al. 2000. Magnetoresistance in ordered and disordered double perovskite oxide, Sr_2FeMoO_6. *Solid State Commun.* 114:465–68
13. Wei F, Deng Z, Sun S, Xie F, Kieslich G, et al. 2016. The synthesis, structure and electronic properties of a lead-free hybrid inorganic–organic double perovskite $(MA)_2KBiCl_6$ (MA = methylammonium). *Mater. Horiz.* 3:328–32
14. Sekiya T, Yamamoto T, Torii Y. 1984. Cation ordering in $(NaLa)(MgW)O_6$ with the perovskite structure. *Bull. Chem. Soc. Jpn.* 57:1859–62
15. Yang M, Oró-Solé J, Rodgers JA, Jorge AB, Fuertes A, Attfield JP. 2011. Anion order in perovskite oxynitrides. *Nat. Chem.* 3:47–52
16. Wu Y, Halat DM, Wei F, Binford T, Seymour ID, et al. 2018. Mixed X-site formate-hypophosphite hybrid perovskites. *Chem. Eur. J.* 24:11309–13
17. Balz D, Plieth K. 1955. Die Struktur des Kaliumnickelfluorids, K_2NiF. *Z. Elektrochem.* 59:545–51
18. Bednorz JG, Müller KA. 1986. Possible high T_c superconductivity in the Ba-La-Cu-O system. *Z. Phys. B* 64:189–93
19. Ruddlesden S, Popper P. 1958. The compound $Sr_3Ti_2O_7$ and its structure. *Acta Crystallogr.* 11:54–55
20. Dion M, Ganne M, Tournoux M. 1981. Nouvelles familles de phases $M^IM_2^{II}Nb_3O_{10}$ a feuillets "perovskites." *Mater. Res. Bull.* 16:1429–35
21. Jacobson A, Johnson JW, Lewandowski J. 1985. Interlayer chemistry between thick transition-metal oxide layers: synthesis and intercalation reactions of $K[Ca_2Na_{n-3}Nb_nO_{3n+1}]$ ($3 \leq n \leq 7$). *Inorg. Chem.* 24:3727–29
22. Smith MD, Crace EJ, Jaffe A, Karunadasa HI. 2018. The diversity of layered halide perovskites. *Annu. Rev. Mater. Res.* 48:111–36
23. Vargas B, Ramos E, Pérez-Gutiérrez E, Alonso JC, Solis-Ibarra D. 2017. A direct bandgap copper–antimony halide perovskite. *J. Am. Chem. Soc.* 139:9116–19
24. Battle PD, Green MA, Laskey NS, Millburn JE, Rosseinsky MJ, et al. 1996. Coupled metal-insulator and magnetic transitions in $LnSr_2Mn_2O_7$ (Ln = La, Tb). *Chem. Commun.* 207:767–68
25. Seshadri R, Martin C, Maignan A, Hervieu M, Raveau B, Rao CNR. 1996. Structure and magnetotransport properties of the layered manganites $RE_{1.2}Sr_{1.8}Mn_2O_7$ (RE = La, Pr, Nd). *J. Mater. Chem.* 6:1585–90
26. Clarke SJ, Hardstone KA, Michie CW, Rosseinsky MJ. 2002. High-temperature synthesis and structures of perovskite and $n = 1$ Ruddlesden-Popper tantalum oxynitrides. *Chem. Mater.* 14:2664–69
27. Connor BA, Leppert L, Smith MD, Neaton JB, Karunadasa HI. 2018. Layered halide double perovskites: dimensional reduction of $Cs_2AgBiBr_6$. *J. Am. Chem. Soc.* 140:5235–40
28. Akamatsu H, Fujita K, Kuge T, Sen Gupta A, Togo A, et al. 2014. Inversion symmetry breaking by oxygen octahedral rotations in the Ruddlesden-Popper $NaRTiO_4$ family. *Phys. Rev. Lett.* 112:187602

29. Kanade K, Baeg J, Kong K, Kale B, Lee S, et al. 2008. A new layer perovskites $Pb_2Ga_2Nb_2O_{10}$ and $RbPb_2Nb_2O_7$: an efficient visible light driven photocatalysts to hydrogen generation. *Int. J. Hydrog. Energy* 33:6904–12
30. Fjellvåg ØS, Armstrong J, Vajeeston P, Sjåstad AO. 2018. New insights into hydride bonding, dynamics, and migration in La_2LiHO_3 oxyhydride. *J. Phys. Chem. Lett.* 9:353–58
31. Park GE, Byeon SH. 1996. Correlation between structures and ionic conductivities of $Na_2Ln_2Ti_3O_{10}$ (Ln = La, Nd, Sm, and Gd). *Bull. Korean Chem. Soc.* 17:168–72
32. Schaak RE, Mallouk TE. 2000. Prying apart Ruddlesden-Popper phases: exfoliation into sheets and nanotubes for assembly of perovskite thin films. *Chem. Mater.* 12:3427–34
33. Ma R, Sasaki T. 2015. Two-dimensional oxide and hydroxide nanosheets: controllable high-quality exfoliation, molecular assembly, and exploration of functionality. *Acc. Chem. Res.* 48:136–43
34. ten Elshof JE, Yuan H, Gonzalez Rodriguez P. 2016. Two-dimensional metal oxide and metal hydroxide nanosheets: synthesis, controlled assembly and applications in energy conversion and storage. *Adv. Energy Mater.* 6:1600355
35. Gönen ZS, Paluchowski D, Zavalij P, Eichhorn BW, Gopalakrishnan J. 2006. Reversible cation/anion extraction from $K_2La_2Ti_3O_{10}$: formation of new layered titanates, $KLa_2Ti_3O_{9.5}$ and $La_2Ti_3O_9$. *Inorg. Chem.* 45:8736–42
36. Toda K, Teranishi T, Ye ZG, Sato M, Hinatsu Y. 1999. Structural chemistry of new ion-exchangeable tantalates with layered perovskite structure: new Dion–Jacobson phase $MCa_2Ta_3O_{10}$ (M = alkali metal) and Ruddlesden–Popper phase $Na_2Ca_2Ta_3O_{10}$. *Mater. Res. Bull.* 34:971–82
37. Hyeon KA, Byeon SH. 1999. Synthesis and structure of new layered oxides, $M^{II}La_2Ti_3O_{10}$ (M = Co, Cu, and Zn). *Chem. Mater.* 11:352–57
38. Fukuoka H, Isami T, Yamanaka S. 2000. Crystal structure of a layered perovskite niobate $KCa_2Nb_3O_{10}$. *J. Solid State Chem.* 151:40–45
39. Thangadurai V, Schmid-Beurmann P, Weppner W. 2001. Synthesis, structure, and electrical conductivity of $A'[A_2B_3O_{10}]$ (A′ = Rb, Cs; A = Sr, Ba; B = Nb, Ta): new members of Dion-Jacobson-type layered perovskites. *J. Solid State Chem.* 158:279–89
40. Anderson MT, Greenwood KB, Taylor GA, Poeppelmeier KR. 1993. B-cation arrangements in double perovskites. *Prog. Solid State Chem.* 22:197–233
41. Toda K, Teranishi T, Takahashi M, Ye ZG, Sato M. 1998. Structural chemistry of new ion-exchangeable tantalates with layered perovskite structure: new reduced Ruddlesden-Popper phase, $Na_2Ca_2Ta_3O_{10}$. *Solid State Ionics* 113-115:501–8
42. Shannon RDT, Prewitt CT. 1969. Effective ionic radii in oxides and fluorides. *Acta Crystallogr. B* 25:925–46
43. Uma S, Gopalakrishnan J. 1993. $K_{1-x}La_xCa_{2-x}Nb_3O_{10}$, a layered perovskite series with variable interlayer cation density, and $LaCaNb_3O_{10}$, a novel layered perovskite oxide with no interlayer cations. *J. Solid State Chem.* 102:332–39
44. Nishimoto S, Matsuda M, Harjo S, Hoshikawa A, Kamiyama T, et al. 2006. Structure determination of $n = 1$ Ruddlesden–Popper compound $HLaTiO_4$ by powder neutron diffraction. *J. Eur. Ceram. Soc.* 26:725–29
45. Chen D, Jiao X, Xu R. 1999. Hydrothermal synthesis and characterization of the layered titanates $MLaTiO_4$ (M = Li, Na, K) powders. *Mater. Res. Bull.* 34:685–91
46. Toda K, Kurita S, Sato M. 1996. New layered perovskite compounds, $LiLaTiO_4$ and $LiEuTiO_4$. *J. Ceram. Soc. Jpn.* 104:140–42
47. Zhu BC, Tang KB. 2011. Rietveld refinement of $KLaTiO_4$ from X-ray powder data. *Acta Crystallogr. E* 67:i26
48. Toda K, Kurita S, Sato M. 1995. Synthesis and ionic conductivity of novel layered perovskite compounds, $AgLaTiO_4$ and $AgEuTiO_4$. *Solid State Ionics* 81:267–71
49. Byeon SH, Park K, Itoh M. 1996. Structure and ionic conductivity of $NaLnTiO_4$; comparison with those of $Na_2Ln_2Ti_3O_{10}$ (Ln = La, Nd, Sm, and Gd). *J. Solid State Chem.* 121:430–36
50. Toda K, Kameo Y, Kurita S, Sato M. 1996. Crystal structure determination and ionic conductivity of layered perovskite compounds $NaLnTiO_4$ (Ln = rare earth). *J. Alloys Compd.* 234:19–25

51. Reddy VR, Hwang DW, Lee JS. 2003. Effect of Zr substitution for Ti in $KLaTiO_4$ for photocatalytic water splitting. *Catal. Lett.* 90:39–43
52. Gupta AS, Akamatsu H, Strayer ME, Lei S, Kuge T, et al. 2016. Improper inversion symmetry breaking and piezoelectricity through oxygen octahedral rotations in layered perovskite family, Li*R*TiO_4 (*R* = rare earths). *Adv. Electron. Mater.* 2:1500196
53. Sen Gupta A, Akamatsu H, Brown FG, Nguyen MAT, Strayer ME, et al. 2017. Competing structural instabilities in the Ruddlesden–Popper derivatives $HRTiO_4$ (R = rare earths): oxygen octahedral rotations inducing noncentrosymmetricity and layer sliding retaining centrosymmetricity. *Chem. Mater.* 29:656–65
54. Akamatsu H, Fujita K, Kuge T, Gupta AS, Rondinelli JM, et al. 2019. *A*-site cation size effect on oxygen octahedral rotations in acentric Ruddlesden-Popper alkali rare-earth titanates. *Phys. Rev. Mater.* 5:065001
55. Su Y, Tsujimoto Y, Fujii K, Tatsuta M, Oka K, et al. 2018. Synthesis, crystal structure, and optical properties of layered perovskite scandium oxychlorides: Sr_2ScO_3Cl, $Sr_3Sc_2O_5Cl_2$, and $Ba_3Sc_2O_5Cl_2$. *Inorg. Chem.* 57:5615–23
56. Kamegashira N, Meng J, Fujita K, Satoh H, Shishido T, Nakajima K. 2006. Study on the phase behavior of $BaEu_2Mn_2O_7$ through heat treatment of a single crystal. *J. Alloys Compd.* 408-412:603–7
57. Armstrong AR, Anderson PA. 1994. Synthesis and structure of a new layered niobium blue bronze: $Rb_2LaNb_2O_7$. *Inorg. Chem.* 33:4366–69
58. Strayer ME, Gupta AS, Akamatsu H, Lei S, Benedek NA, et al. 2016. Emergent noncentrosymmetry and piezoelectricity driven by oxygen octahedral rotations in $n = 2$ Dion-Jacobson phase layer perovskites. *Adv. Funct. Mater.* 26:1930–37
59. Kumada N, Kinomura N, Sleight AW. 1996. $CsLaNb_2O_7$. *Acta Crystallogr. C* 52:1063–65
60. Toda K, Sato M. 1996. Synthesis and structure determination of new layered perovskite compounds, $ALaTa_2O_7$ and $ACa_2Ta_3O_{10}$ (*A* = Rb, Li). *J. Mater. Chem.* 6:1067–71
61. Subramanian M, Gopalakrishnan J, Sleight A. 1988. New layered perovskites: $ABiNb_2O_7$ and $APb_2Nb_3O_{10}$ (A = Rb or Cs). *Mater. Res. Bull.* 23:837–42
62. Goff RJ, Keeble D, Thomas PA, Ritter C, Morrison FD, Lightfoot P. 2009. Leakage and proton conductivity in the predicted ferroelectric $CsBiNb_2O_7$. *Chem. Mater.* 21:1296–302
63. Snedden A, Knight KS, Lightfoot P. 2003. Structural distortions in the layered perovskites $CsANb_2O_7$ (A = Nd, Bi). *J. Solid State Chem.* 173:309–13
64. Benedek NA. 2014. Origin of ferroelectricity in a family of polar oxides: the Dion-Jacobson phases. *Inorg. Chem.* 53:3769–77
65. Mulder AT, Benedek NA, Rondinelli JM, Fennie CJ. 2013. Turning ABO_3 antiferroelectrics into ferroelectrics: design rules for practical rotation-driven ferroelectricity in double perovskites and $A_3B_2O_7$ Ruddlesden-Popper compounds. *Adv. Funct. Mater.* 23:4810–20
66. Zhang R, Abbett BM, Read G, Lang F, Lancaster T, et al. 2016. $La_2SrCr_2O_7$: controlling the tilting distortions of $n = 2$ Ruddlesden–Popper phases through A-site cation order. *Inorg. Chem.* 55:8951–60
67. Zhu T, Cohen T, Gibbs AS, Zhang W, Halasyamani PS, et al. 2017. Theory and neutrons combine to reveal a family of layered perovskites without inversion symmetry. *Chem. Mater.* 29:9489–97
68. Zhu T, Khalsa G, Havas DM, Gibbs AS, Zhang W, et al. 2018. Cation exchange as a mechanism to engineer polarity in layered perovskites. *Chem. Mater.* 30:8915–24
69. Autieri C, Barone P, Sławińska J, Picozzi S. 2019. Persistent spin helix in Rashba-Dresselhaus ferroelectric $CsBiNb_2O_7$. *Phys. Rev. Mater.* 3:084416
70. Honma T, Toda K, Ye ZG, Sato M. 1998. Concentration quenching of the Eu^{3+} -activated luminescence in some layered perovskites with two-dimensional arrangement. *J. Phys. Chem. Solids* 59:1187–93
71. Argyriou DN, Bordallo HN, Campbell BJ, Cheetham AK, Cox DE, et al. 2000. Charge ordering and phase competition in the layered perovskite $LaSr_2Mn_2O_7$. *Phys. Rev. B* 61:15269–76
72. Zhou G, Jiang X, Zhao J, Molokeev M, Lin Z, et al. 2018. Two-dimensional-layered perovskite $ALaTa_2O_7$: Bi^{3+} (A = K and Na) phosphors with versatile structures and tunable photoluminescence. *ACS Appl. Mater. Interfaces* 10:24648–55
73. Liang Z, Tang K, Shao Q, Li G, Zeng S, Zheng H. 2008. Synthesis, crystal structure, and photocatalytic activity of a new two-layer Ruddlesden–Popper phase, $Li_2CaTa_2O_7$. *J. Solid State Chem.* 181:964–70

74. Galven C, Mounier D, Bouchevreau B, Suard E, Bulou A, et al. 2016. Phase transitions in the Ruddlesden–Popper phase $Li_2CaTa_2O_7$: X-ray and neutron powder thermodiffraction, TEM, Raman, and SHG experiments. *Inorg. Chem.* 55:2309–23
75. Zhang W, Fujii K, Niwa E, Hagihala M, Kamiyama T, Yashima M. 2020. Oxide-ion conduction in the Dion-Jacobson phase $CsBi_2Ti_2NbO_{10-\delta}$. *Nat. Commun.* 11:1224
76. Kim HG, Tran TT, Choi W, You TS, Halasyamani PS, Ok KM. 2016. Two new non-centrosymmetric $n = 3$ layered Dion-Jacobson perovskites: polar $RbBi_2Ti_2NbO_{10}$ and nonpolar $CsBi_2Ti_2TaO_{10}$. *Chem. Mater.* 28:2424–32
77. Acosta M, Novak N, Rojas V, Patel S, Vaish R, et al. 2017. $BaTiO_3$-based piezoelectrics: fundamentals, current status, and perspectives. *Appl. Phys. Rev.* 4:041305
78. Zahedi E, Hojamberdiev M, Bekheet MF. 2015. Electronic, optical and photocatalytic properties of three-layer perovskite Dion-Jacobson phase $CsBa_2M_3O_{10}$ (M = Ta, Nb): a DFT study. *RSC Adv.* 5:88725–35
79. Gopalakrishnan J, Sivakumar T, Thangadurai V, Subbanna GN. 1999. $A[Bi_3Ti_4O_{13}]$ and $A[Bi_3PbTi_5O_{16}]$ (A = K, Cs): new $n = 4$ and $n = 5$ members of the layered perovskite series, $A[A'_{n-1}B_nO_{3n+1}]$, and their hydrates. *Inorg. Chem.* 38:2802–6
80. Zong X, Sun C, Chen Z, Mukherji A, Wu H, et al. 2011. Nitrogen doping in ion-exchangeable layered tantalate towards visible-light induced water oxidation. *Chem. Commun.* 47:6293
81. Maeda K, Eguchi M, Oshima T. 2014. Perovskite oxide nanosheets with tunable band-edge potentials and high photocatalytic hydrogen-evolution activity. *Angew. Chem. Int. Ed.* 53:13164–68
82. Sato M, Toda K, Watanabe J, Uematsu K. 1993. Structure determination and silver ion conductivity of layered perovskite compounds $M_2La_2Ti_3O_{10}$ (M = K and Ag). *Nippon Kagaku Kaishi* 1993:640–46
83. Rodionov IA, Silyukov OI, Utkina TD, Chislov MV, Sokolova YP, Zvereva IA. 2012. Photocatalytic properties and hydration of perovskite-type layered titanates $A_2Ln_2Ti_3O_{10}$ (A = Li, Na, K; Ln = La, Nd). *Russ. J. Gen. Chem.* 82:1191–96
84. Gustin L, Hosaka Y, Tassel C, Aharen T, Shimakawa Y, et al. 2016. From tetrahedral to octahedral iron coordination: layer compression in topochemically prepared $FeLa_2Ti_3O_{10}$. *Inorg. Chem.* 55:11529–37
85. Pratt JA, Shepherd AM, Hayward MA. 2015. Diamagnetic Ru^{2+} in $Na_2La_2Ti_2RuO_{10-x}$ ($0 < x < 2$): a series of complex oxides prepared by topochemical reduction. *Inorg. Chem.* 54:10993–97
86. Schaak RE, Guidry EN, Mallouk TE. 2001. Converting a layer perovskite into a non-defective higher-order homologue: topochemical synthesis of $Eu_2CaTi_2O_7$. *Chem. Commun.* 2001:853–54
87. Thangadurai V, Gopalakrishnan J, Subbanna GN. 1998. $Ln_2Ti_2O_7$ (Ln = La, Nd, Sm, Gd): a novel series of defective Ruddlesden-Popper phases formed by topotactic dehydration of $HLnTiO_4$. *Chem. Commun.* 7:1299–300
88. Abou-Warda S, Pietzuch W, Berghöfer G, Kesper U, Massa W, Reinen D. 1998. Ordered K_2NiF_4 structure of the solids $La_2Li_{1/2}M_{1/2}O_4$ (M(III) = Co, Ni, Cu) and the bonding properties of the MO_6 polyhedra in various compounds of this type. *J. Solid State Chem.* 138:18–31
89. Abbattista F, Vallino M, Mazza D. 1985. Preparation and crystallographic characteristics of the new phase $La_2Au_{0.5}Li_{0.5}O_4$. *J. Less Common Met.* 110:391–96
90. Lehner AJ, Fabini DH, Evans HA, Hébert CA, Smock SR, et al. 2015. Crystal and electronic structures of complex bismuth iodides $A_3Bi_2I_9$ (A = K, Rb, Cs) related to perovskite: aiding the rational design of photovoltaics. *Chem. Mater.* 27:7137–48
91. Teneze N, Mercurio D, Trolliard G, Frit B. 2000. Cation-deficient perovskite-related compounds $(Ba,La)_n$ $Ti_{n-1}O_{3n}$ ($n = 4$, 5, and 6): a Rietveld refinement from neutron powder diffraction data. *Mater. Res. Bull.* 35:1603–14
92. Kemmler-Sack S, Wischert W, Treiber U. 1978. Über hexagonale Perowskite mit Kationenfehlstellen. III. Strukturbestimmungen an Verbindungen vom Typ $Ba_2B_{1/3}{}^{III}{}_{2/3}Re^{VII}O_6$. *Z. Anorg. Allg. Chem.* 444:190–94
93. Yu R, Fan A, Li T, Yuan M, Wang J. 2017. Structure and luminescence properties of Eu^{3+}-doped trigonal double-perovskite $Ba_2Lu_{0.667}WO_6$. *Mater. Chem. Phys.* 196:75–81
94. Longo JM, Katz L, Ward R. 1965. Rhenium-containing complex metal oxides of the formula type $A^{II}{}_4Re^{VII}{}_2M^{II}O_{12}$. *Inorg. Chem.* 4:235–41

95. Herrmann M, Kemmler-Sack S. 1980. Über hexagonale Perowskite mit Kationenfehlstellen. XXII. Die Polymorphie bei rhomboedrischen 12 L-Stapelvarianten im System $Sr_{4-x}Ba_xNiRe_2O_{12}$. *Z. Anorg. Allg. Chem.* 469:51–60
96. Rawl R, Lee M, Choi ES, Li G, Chen KW, et al. 2017. Magnetic properties of the triangular lattice magnets $A_4B'B_2O_{12}$ (A = Ba, Sr, La; B′ = Co, Ni, Mn; B = W, Re). *Phys. Rev. B* 95:174438
97. Rother H, Kemmler-Sack S. 1980. Uber hexagonale Perowskite mit Kationenfehlstellen. XIX. Die rhomboedrischen 12 L-Stapelvarianten vom Typ Ba_3LaB^{III} (W_2VIO_{12}). *Z. Anorg. Allg. Chem.* 465:179–82
98. Falk F, Hackbarth L, Lochbrunner S, Marciniak H, Küppers T, Köckerling M. 2018. Rare-earth metal tetracyanidoborate hydrate salts: structural, spectral, and thermal properties as well as the luminescence of dehydrated salts. *Z. Anorg. Allg. Chem.* 644:1495–502
99. Saito M, Watanabe M, Kurita N, Matsuo A, Kindo K, et al. 2019. Successive phase transitions and magnetization plateau in the spin-1 triangular-lattice antiferromagnet $Ba_2La_2NiTe_2O_{12}$ with small easy-axis anisotropy. *Phys. Rev. B* 100:064417
100. Doi Y, Wakeshima M, Tezuka K, Shan YJ, Ohoyama K, et al. 2017. Crystal structures, magnetic properties, and DFT calculation of B-site defected 12L-perovskites $Ba_2La_2MW_2O_{12}$ (M = Mn, Co, Ni, Zn). *J. Condens. Matter Phys.* 29:365802
101. Li Z, Sun J, Wang Y, You L, Lin JH. 2005. Structural and magnetic properties of $Ba_3La_3Mn_2W_3O_{18}$. *J. Solid State Chem.* 178:114–19
102. Kim SW, Zhang R, Halasyamani PS, Hayward MA. 2015. $K_4Fe_3F_{12}$: an Fe^{2+}/Fe^{3+} charge-ordered, ferrimagnetic fluoride with a cation-deficient, layered perovskite structure. *Inorg. Chem.* 54:6647–52
103. Liu S, Xu Y, Qu N, Zhang Y, Wang J, et al. 2017. Charge ordering in $K_4Fe_3F_{12}$ from a first principles study. *ChemistrySelect* 2:714–19
104. Frenzen G, Kummer S, Massa W, Babel D. 1987. Tetragonale Fluorperowskite $AM_{0,750}\,\square_{\,0,25}F_3$ mit Kationendefizit: $K_4Mn^{II}Mn_2{}^{III}F_{12}$ und $Ba_2Cs_2Cu_3F_{12}$. *Z. Anorg. Allg. Chem.* 553:75–84
105. Manaka H, Miyashita Y, Watanabe Y, Masuda T. 2007. Synthesis of double-layer perovskite fluoride $K_3Cu_2F_7$ with spin gap and orbital order. *J. Phys. Soc. Jpn.* 76:044710
106. Herdtweck E, Babel D. 1981. Röntgenographische Einkristallstrukturbestimmungen an den Kalium-Kupfer(II)-Fluoriden K_2CuF_4 und $K_3Cu_2F_7$. *Z. Anorg. Allg. Chem.* 474:113–22
107. Herdtweck E, Kummer S, Babel D. 1991. Cation-deficient perovskites $Ba_2A^IM_2{}^{II}F_9$ (M^{II} = Fe, Co, Ni, Zn) and their hexagonal layer structure. *Eur. J. Solid State Inorg. Chem.* 28:959–69
108. Vargas B, Torres-Cadena R, Rodríguez-Hernández J, Gembicky M, Xie H, et al. 2018. Optical, electronic, and magnetic engineering of <111> layered halide perovskites. *Chem. Mater.* 30:5315–21
109. Tang G, Xiao Z, Hosono H, Kamiya T, Fang D, Hong J. 2018. Layered halide double perovskites $Cs_{3+n}M(II)_nSb_2X_{9+3n}$ (M = Sn, Ge) for photovoltaic applications. *J. Phys. Chem. Lett.* 9:43–48
110. Xu J, Liu JB, Wang J, Liu BX, Huang B. 2018. Prediction of novel p-type transparent conductors in layered double perovskites: a first-principles study. *Adv. Funct. Mater.* 28:1800332
111. Liu Z, Zhao X, Zunger A, Zhang L. 2019. Design of mixed-cation tri-layered Pb-free halide perovskites for optoelectronic applications. *Adv. Electron. Mater.* 5:1900234
112. Li J, Yu Q, He Y, Stoumpos CC, Niu G, et al. 2018. $Cs_2PbI_2Cl_2$, all-inorganic two-dimensional Ruddlesden-Popper mixed halide perovskite with optoelectronic response. *J. Am. Chem. Soc.* 140:11085–90
113. Li J, Stoumpos CC, Trimarchi GG, Chung I, Mao L, et al. 2018. Air-stable direct bandgap perovskite semiconductors: all-inorganic tin-based heteroleptic halides $A_xSnCl_yI_z$ (A = Cs, Rb). *Chem. Mater.* 30:4847–56
114. Xu Z, Chen M, Liu SF. 2019. Layer-dependent ultrahigh-mobility transport properties in all-inorganic two-dimensional $Cs_2PbI_2Cl_2$ and $Cs_2SnI_2Cl_2$ perovskites. *J. Phys. Chem. C* 123:27978–85
115. McCall KM, Stoumpos CC, Kontsevoi OY, Alexander GCB, Wessels BW, Kanatzidis MG. 2019. From 0D $Cs_3Bi_2I_9$ to 2D $Cs_3Bi_2I_6Cl_3$: Dimensional expansion induces a direct band gap but enhances electron–phonon coupling. *Chem. Mater.* 31:2644–50
116. Morgan EE, Mao L, Teicher SML, Wu G, Seshadri R. 2020. Tunable perovskite-derived bismuth halides: $Cs_3Bi_2\ (Cl_{1-x}I_x)_9$. *Inorg. Chem.* 59:3387–93

117. Hodgkins TL, Savory CN, Bass KK, Seckman BL, Scanlon DO, et al. 2019. Anionic order and band gap engineering in vacancy ordered triple perovskites. *Chem. Commun.* 55:3164–67
118. Kobayashi Y, Tsujimoto Y, Kageyama H. 2018. Property engineering in perovskites via modification of anion chemistry. *Annu. Rev. Mater. Res.* 48:303–26
119. Harada JK, Charles N, Poeppelmeier KR, Rondinelli JM. 2019. Heteroanionic materials by design: progress toward targeted properties. *Adv. Mater.* 31:1805295
120. Fuertes A. 2006. Prediction of anion distributions using Pauling's second rule. *Inorg. Chem.* 45:9640–42
121. Loureiro SM, Felser C, Huang Q, Cava RJ. 2000. Refinement of the crystal structures of strontium cobalt oxychlorides by neutron powder diffraction. *Chem. Mater.* 12:3181–85
122. Tsujimoto Y, Yamaura K, Uchikoshi T. 2013. Extended Ni(III) oxyhalide perovskite derivatives: Sr_2NiO_3X (X = F, Cl). *Inorg. Chem.* 52:10211–16
123. Knee CS, Weller MT. 2002. New layered manganese oxide halides. *Chem. Commun.* 2:256–57
124. Romero FD, Hayward MA. 2012. Structure and magnetism of the topotactically reduced oxychloride $Sr_4Mn_3O_{6.5}Cl_2$. *Inorg. Chem.* 51:5325–31
125. Su Y, Tsujimoto Y, Fujii K, Tatsuta M, Oka K, et al. 2018. Synthesis, crystal structure, and optical properties of layered perovskite scandium oxychlorides: Sr_2ScO_3Cl, $Sr_3Sc_2O_5Cl_2$, and $Ba_3Sc_2O_5Cl_2$. *Inorg. Chem.* 57:5615–23
126. Yoo CY, Kim J, Kim SC, Kim SJ. 2018. Crystal structures of new layered perovskite-type oxyfluorides, $CsANb_2O_6F$ (A = Sr and Ca) and comparison with pyrochlore-type $CsNb_2O_5F$. *J. Solid State Chem.* 267:146–52
127. Tsujimoto Y, Yamaura K, Takayama-Muromachi E. 2012. Oxyfluoride chemistry of layered perovskite compounds. *Appl. Sci.* 2:206–19
128. Harada JK, Poeppelmeier KR, Rondinelli JM. 2019. Predicting the structure stability of layered heteroanionic materials exhibiting anion order. *Inorg. Chem.* 58:13229–40
129. Wang Y, Tang K, Zhu B, Wang D, Hao Q, Wang Y. 2015. Synthesis and structure of a new layered oxyfluoride Sr_2ScO_3F with photocatalytic property. *Mater. Res. Bull.* 65:42–46
130. Choy JH, Kim JY, Kim SJ, Sohn JS, Han OH. 2001. New Dion-Jacobson-type layered perovskite oxyfluorides, $ASrNb_2O_6F$ (A = Li, Na, and Rb). *Chem. Mater.* 13:906–12
131. Su Y, Tsujimoto Y, Matsushita Y, Yuan Y, He J, Yamaura K. 2016. High-pressure synthesis, crystal structure, and magnetic properties of Sr_2MnO_3F: a new member of layered perovskite oxyfluorides. *Inorg. Chem.* 55:2627–33
132. Kobayashi Y, Tian M, Eguchi M, Mallouk TE. 2009. Ion-exchangeable, electronically conducting layered perovskite oxyfluorides. *J. Am. Chem. Soc.* 131:9849–55
133. Needs RL, Weller MT. 1995. Synthesis and structure of Ba_2InO_3F: oxide/fluoride ordering in a new K_2NiF_4 superstructure. *Chem. Commun.* 7:353–54
134. Tarasova NA, Animitsa IE. 2018. The influence of the nature of halogen on the local structure and intercalation of water in oxyhalides Ba_2InO_3X (X = F, Cl, Br). *Opt. Spectrosc.* 124:163–66
135. Needs RL, Weller MT, Scheler U, Harris RK. 1996. Synthesis and structure of Ba_2InO_3X (X = F, Cl, Br) and Ba_2ScO_3F; oxide/halide ordering in K_2NiF_4-type structures. *J. Mater. Chem.* 6:1219–24
136. Galasso F, Darby W. 1963. Preparation and properties of Sr_2FeO_3F. *J. Phys. Chem.* 67:1451–53
137. Case GS, Hector AL, Levason W, Needs RL, Thomas MF, Weller MT. 1999. Syntheses, powder neutron diffraction structures and Mössbauer studies of some complex iron oxyfluorides: $Sr_3Fe_2O_6F_{0.87}$, Sr_2FeO_3F and $Ba_2InFeO_5F_{0.68}$. *J. Mater. Chem.* 9:2821–27
138. Hector AL, Hutchings JA, Needs RL, Thomas MF, Weller MT. 2001. Structural and Mössbauer study of Sr_2FeO_3X (X = F, Cl, Br) and the magnetic structure of Sr_2FeO_3F. *J. Mater. Chem.* 11:527–32
139. Yoo CY, Hong KP, Kim SJ. 2007. A new layered perovskite, $KSrNb_2O_6F$, by powder neutron diffraction. *Acta Crystallogr. C* 63:i63–65
140. Subramanian M, Aravamudan G, Subba Rao G. 1983. Oxide pyrochlores—a review. *Prog. Solid State Chem.* 15:55–143
141. Yoo CY, Kim SJ. 2008. Dimensional modification of oxyfluoride lattice: preparation and structure of $A'ANb_2O_6F$ (A′ = Na, K, A = Ca, Sr). *J. Phys. Chem. Solids* 69:1475–78

142. Hector AL, Knee CS, MacDonald AI, Price DJ, Weller MT. 2005. An unusual magnetic structure in Sr_2FeO_3F and magnetic structures of K_2NiF_4-type iron(III) oxides and oxide halides, including the cobalt substituted series $Sr_2Fe_{1-x}Co_xO_3Cl$. *J. Mater. Chem.* 15:3093–103
143. Knee CS, Zhukov AA, Weller MT. 2002. Crystal structures and magnetic properties of the manganese oxide chlorides Sr_2MnO_3Cl and $Sr_4Mn_3O_{8-y}Cl_2$. *Chem. Mater.* 14:4249–55
144. Ronning F, Kim C, Feng DL, Marshall DS, Loeser AG, et al. 1998. Photoemission evidence for a remnant Fermi surface and a d-wave-like dispersion in insulating $Ca_2CuO_2Cl_2$. *Science* 282:2067–72
145. Kohsaka Y, Azuma M, Yamada I, Sasagawa T, Hanaguri T, et al. 2002. Growth of Na-doped $Ca_2CuO_2Cl_2$ single crystals under high pressures of several GPa. *J. Am. Chem. Soc.* 124:12275–78
146. Muller-Buschbaum H, Boje J. 1991. Zur Kenntnis eines Halogenooxo-Cobaltats(III): $Sr_8Co_6O_{15}Cl_4$. *Z. Anorg. Allg. Chem.* 592:73–78
147. Vaknin D, Miller LL, Zarestky JL. 1997. Stacking of the square-lattice antiferromagnetic planes in $Ca_2CuO_2Cl_2$. *Phys. Rev. B* 56:8351–59
148. Knee CS, Weller MT. 2002. Synthesis and structure of cobalt(II) oxide halides—$Sr_2CoO_2X_2$ (X = Cl, Br). *J. Solid State Chem.* 168:1–4
149. Knee CS, Weller MT. 2003. Synthesis and structure of new layered copper oxide iodides, $Sr_2CuO_2I_2$ and $Sr_2Cu_3O_4I_2$. *J. Mater. Chem.* 13:1507–9
150. Lafond A, Leynaud O, André G, Bourée F, Meerschaut A. 2002. Magnetic properties of $Ln_2Ti_2S_2O_5$ compounds and magnetic structure of $Tb_2Ti_2S_2O_5$. *J. Alloys Compd.* 338:185–93
151. Yashima M, Ogisu K, Domen K. 2008. Structure and electron density of oxysulfide $Sm_2Ti_2S_2O_{4.9}$, a visible-light-responsive photocatalyst. *Acta Crystallogr. B* 64:291–98
152. Goga M, Seshadri R, Ksenofontov V, Gütlich P, Tremel W. 1999. $Ln_2Ti_2S_2O_5$ (Ln = Nd, Pr, Sm): a novel series of defective Ruddlesden–Popper phases. *Chem. Commun.* 2006:979–80
153. Rutt OJ, Hill TL, Gál ZA, Hayward MA, Clarke SJ. 2003. The cation-deficient Ruddlesden-Popper oxysulfide $Y_2Ti_2O_5S_2$ as a layered sulfide: topotactic potassium intercalation to form $KY_2Ti_2O_5S_2$. *Inorg. Chem.* 42:7906–11
154. Wang Q, Nakabayashi M, Hisatomi T, Sun S, Akiyama S, et al. 2019. Oxysulfide photocatalyst for visible-light-driven overall water splitting. *Nat. Mater.* 18:827–32
155. Fuertes A. 2015. Metal oxynitrides as emerging materials with photocatalytic and electronic properties. *Mater. Horiz.* 2:453–61
156. Wu Y, Lazic P, Hautier G, Persson K, Ceder G. 2013. First principles high throughput screening of oxynitrides for water-splitting photocatalysts. *Energy Environ. Sci.* 6:157–68
157. Fuertes A. 2012. Chemistry and applications of oxynitride perovskites. *J. Mater. Chem.* 22:3293–99
158. Oshima T, Ichibha T, Qin KS, Muraoka K, Vequizo JJM, et al. 2018. Undoped layered perovskite oxynitride $Li_2LaTa_2O_6N$ for photocatalytic CO_2 reduction with visible light. *Angew. Chem.* 130:8286–90
159. Diot N, Marchand R, Haines J, Léger J, Macaudière P, Hull S. 1999. Crystal structure determination of the oxynitride Sr_2TaO_3N. *J. Solid State Chem.* 146:390–93
160. Tobías G, Oró-Solé J, Beltrán-Porter D, Fuertes A. 2001. New family of Ruddlesden-Popper strontium niobium oxynitrides: $(SrO)(SrNbO_{2-x}N)_n$ ($n = 1, 2$). *Inorg. Chem.* 40:6867–69
161. Bouri M, Aschauer U. 2018. Bulk and surface properties of the Ruddlesden–Popper oxynitride Sr_2TaO_3N. *Phys. Chem. Chem. Phys.* 20:2771–76
162. Wei S, Xu X. 2018. Boosting photocatalytic water oxidation reactions over strontium tantalum oxynitride by structural laminations. *Appl. Catal. B* 228:10–18
163. Tobías G, Beltrán-Porter D, Lebedev OI, Van Tendeloo G, Rodríguez-Carvajal J, Fuertes A. 2004. Anion ordering and defect structure in Ruddlesden-Popper strontium niobium oxynitrides. *Inorg. Chem.* 43:8010–17
164. Kim YI, Woodward PM, Baba-Kishi KZ, Tai CW. 2004. Characterization of the structural, optical, and dielectric properties of oxynitride perovskites AMO_2N (A = Ba, Sr, Ca; M = Ta, Nb). *Chem. Mater.* 16:1267–76
165. Cordes N, Nentwig M, Eisenburger L, Oeckler O, Schnick W. 2019. Ammonothermal synthesis of the mixed-valence nitrogen-rich europium tantalum Ruddlesden-Popper phase $Eu^{II}Eu_2^{III}Ta_2N_4O_3$. *Eur. J. Inorg. Chem.* 2019:2304–11

166. Marchand R. 1982. Structure cristalline de Nd_2AlO_3N. Détermination de l'ordre oxygène-azote par diffraction de neutrons. *Rev. Chim. Miner.* 19:684–89
167. Pelloquin D, Hadermann J, Giot M, Caignaert V, Michel C, et al. 2004. Novel, oxygen-deficient $n = 3$ RP-member $Sr_3NdFe_3O_{9-\delta}$ and its topotactic derivatives. *Chem. Mater.* 16:1715–24
168. Raveau B, Hervieu M, Pelloquin D, Michel C, Retoux R. 2005. A large family of iron Ruddlesden-Popper relatives: from oxides to oxycarbonates and oxyhydroxides. *Z. Anorg. Allg. Chem.* 631:1831–39
169. Jantsky L, Okamoto H, Demont A, Fjellvåg H. 2012. Tuning of water and hydroxide content of intercalated Ruddlesden-Popper-type oxides in the $PrSr_3Co_{1.5}Fe_{1.5}O_{10-\delta}$ system. *Inorg. Chem.* 51:9181–91
170. Pelloquin D, Barrier N, Flahaut D, Caignaert V, Maignan A. 2005. Two new hydrated oxyhydroxides $Sr_3Co_{1.7}Ti_{0.3}O_5$ $(OH)_2xH_2O$ and $Sr_4Co_{1.6}Ti_{1.4}O_8$ $(OH)_2xH_2O$ derived from the RP $n = 2$ and 3 members: structural and magnetic behavior versus temperature. *Chem. Mater.* 17:773–80
171. Motohashi T, Raveau B, Caignaert V, Pralong V, Hervieu M, et al. 2005. Spin glass to weak ferromagnetic transformation in a new layered cobaltite: consequence of topotactic reactions with water at room temperature. *Chem. Mater.* 17:6256–62
172. Bang J, Matsuishi S, Hiraka H, Fujisaki F, Otomo T, et al. 2014. Hydrogen ordering and new polymorph of layered perovskite oxyhydrides: $Sr_2VO_{4-x}H_x$. *J. Am. Chem. Soc.* 136:7221–24
173. Hayward MA. 2002. The hydride anion in an extended transition metal oxide array: $LaSrCoO_3H_{0.7}$. *Science* 295:1882–84
174. Hernandez OJ, Geneste G, Yajima T, Kobayashi Y, Okura M, et al. 2018. Site selectivity of hydride in early-transition-metal Ruddlesden–Popper oxyhydrides. *Inorg. Chem.* 57:11058–67
175. Schwarz H. 1991. *Neuartige Hydrid-Oxide der Seltenen Erden: Ln_2LiHO_3 mit Ln*. Diss., Inst. Anorg. Chem.
176. Kobayashi G, Hinuma Y, Matsuoka S, Watanabe A, Iqbal M, et al. 2016. Pure H-conduction in oxyhydrides. *Science* 351:1314–17
177. Minervini L, Grimes RW, Kilner JA, Sickafus KE. 2000. Oxygen migration in $La_2NiO_{4+\delta}$. *J. Mater. Chem.* 10:2349–54
178. Numata Y, Sanehira Y, Ishikawa R, Shirai H, Miyasaka T. 2018. Thiocyanate containing two-dimensional cesium lead iodide perovskite, $Cs_2PbI_2(SCN)_2$: characterization, photovoltaic application, and degradation mechanism. *ACS Appl. Mater. Interfaces* 10:42363–71
179. Chiang YH, Li MH, Cheng HM, Shen PS, Chen P. 2017. Mixed cation thiocyanate-based pseudohalide perovskite solar cells with high efficiency and stability. *ACS Appl. Mater. Interfaces* 9:2403–9
180. Labram J, Venkatesan N, Takacs C, Evans H, Perry E, et al. 2017. Charge transport in a two-dimensional hybrid metal halide thiocyanate compound. *J. Mater. Chem. C* 5:5930–38
181. Headspith DA, Sullivan E, Greaves C, Francesconi MG. 2009. Synthesis and characterisation of the quaternary nitride-fluoride $Ce_2MnN_3F_{2-\delta}$. *Dalton Trans.* 2009:9273–79
182. Nazarenko O, Kotyrba MR, Wörle M, Cuervo-Reyes E, Yakunin S, Kovalenko MV. 2017. Luminescent and photoconductive layered lead halide perovskite compounds comprising mixtures of cesium and guanidinium cations. *Inorg. Chem.* 56:11552–64
183. Soe CMM, Stoumpos CC, Kepenekian M, Traoré B, Tsai H, et al. 2017. New type of 2D perovskites with alternating cations in the interlayer space, $(C(NH_2)_3)(CH_3NH_3)_nPb_nI_{3n+1}$: structure, properties, and photovoltaic performance. *J. Am. Chem. Soc.* 139:16297–309
184. McNulty JA, Lightfoot P. 2020. Unprecedented tin iodide perovskite-like structures featuring ordering of organic moieties. *Chem. Commun.* 56:4543–46
185. Guo YY, McNulty JA, Mica NA, Samuel IDW, Slawin AMZ, et al. 2019. Structure-directing effects in (110)-layered hybrid perovskites containing two distinct organic moieties. *Chem. Commun.* 55:9935–38
186. Salah MBH, Mercier N, Allain M, Zouari N, Giovanella U, Botta C. 2019. Mechanochromic and electroluminescence properties of a layered hybrid perovskite belonging to the <110> series. *Eur. J. Inorg. Chem.* 2019:4527–31
187. Guo YY, Yang LJ, Biberger S, McNulty JA, Li T, et al. 2020. Structural diversity in layered hybrid perovskites, A_2PbBr_4 or $AA'PbBr_4$, templated by small disc-shaped amines. *Inorg. Chem.* 59:12858–66
188. Nazarenko O, Kotyrba MR, Yakunin S, Aebli M, Rainò G, et al. 2018. Guanidinium-formamidinium lead iodide: a layered perovskite-related compound with red luminescence at room temperature. *J. Am. Chem. Soc.* 140:3850–53

189. Daub M, Hillebrecht H. 2018. First representatives of (210)-oriented perovskite variants—synthesis, crystal structures and properties of the new 2D hybrid perovskites $A[HC(NH_2)_2]PbI_4$; A = $[C(NH_2)_3]$, $[HSC(NH_2)_2]$. *Z. Kristallogr. Cryst. Mater.* 233:555–64
190. Mao L, Stoumpos CC, Kanatzidis MG. 2019. Two-dimensional hybrid halide perovskites: principles and promises. *J. Am. Chem. Soc.* 141:1171–90
191. Mercier N. 2019. Hybrid halide perovskites: discussions on terminology and materials. *Angew. Chem. Int. Ed.* 58:17912–17
192. Smith MD, Connor BA, Karunadasa HI. 2019. Tuning the luminescence of layered halide perovskites. *Chem. Rev.* 119:3104–39
193. Fu Y, Hautzinger MP, Luo Z, Wang F, Pan D, et al. 2019. Incorporating large A cations into lead iodide perovskite cages: relaxed Goldschmidt tolerance factor and impact on exciton–phonon interaction. *ACS Cent. Sci.* 5:1377–86
194. Hautzinger MP, Pan D, Pigg AK, Fu Y, Morrow DJ, et al. 2020. Band edge tuning of two-dimensional Ruddlesden-Popper perovskites by A cation size revealed through nanoplates. *ACS Energy Lett.* 5:1430–37
195. Kieslich G, Sun S, Cheetham AK. 2015. An extended tolerance factor approach for organic–inorganic perovskites. *Chem. Sci.* 6:3430–33
196. Fu Y, Jiang X, Li X, Traore B, Spanopoulos I, et al. 2020. Cation engineering in two-dimensional Ruddlesden-Popper lead iodide perovskites with mixed large A-site cations in the cages. *J. Am. Chem. Soc.* 142:4008–21
197. Liang M, Lin W, Lan Z, Meng J, Zhao Q, et al. 2020. Electronic structure and trap states of two-dimensional Ruddlesden-Popper perovskites with the relaxed Goldschmidt tolerance factor. *ACS Appl. Electron. Mater.* 2:1402–12
198. Li X, Fu Y, Pedesseau L, Guo P, Cuthriell S, et al. 2020. Negative pressure engineering with large cage cations in 2D halide perovskites causes lattice softening. *J. Am. Chem. Soc.* 142:11486–96
199. Jana MK, Janke SM, Dirkes DJ, Dovletgeldi S, Liu C, et al. 2019. Direct-bandgap 2D silver–bismuth iodide double perovskite: the structure-directing influence of an oligothiophene spacer cation. *J. Am. Chem. Soc.* 141:7955–64
200. Bi LY, Hu YQ, Li MQ, Hu TL, Zhang HL, et al. 2019. Two-dimensional lead-free iodide-based hybrid double perovskites: crystal growth, thin-film preparation and photocurrent responses. *J. Mater. Chem. A* 7:19662–67
201. Bi LY, Hu TL, Li MQ, Ling BK, Lassoued MS, et al. 2020. Template effects in Cu(I)–Bi(III) iodide double perovskites: a study of crystal structure, film orientation, band gap and photocurrent response. *J. Mater. Chem. A* 8:7288–96
202. Mao L, Teicher SML, Stoumpos CC, Kennard RM, DeCrescent RA, et al. 2019. Chemical and structural diversity of hybrid layered double perovskite halides. *J. Am. Chem. Soc.* 141:19099–109
203. McClure ET, McCormick AP, Woodward PM. 2020. Four lead-free layered double perovskites with the $n = 1$ Ruddlesden-Popper structure. *Inorg. Chem.* 59:6010–17
204. Guo W, Liu X, Han S, Liu Y, Xu Z, et al. 2020. Room-temperature ferroelectric material composed of a two-dimensional metal halide double perovskite for X-ray detection. *Angew. Chem. Int. Ed.* 59:13879–84
205. Connor BA, Biega RI, Leppert L, Karunadasa HI. 2020. Dimensional reduction of the small-bandgap double perovskite $Cs_2AgTlBr_6$. *Chem. Sci.* 11:7708–15
206. Xu Z, Liu X, Li Y, Liu X, Yang T, et al. 2019. Exploring lead-free hybrid double perovskite crystals of $(BA)_2CsAgBiBr_7$ with large mobility-lifetime product toward X-ray detection. *Angew. Chem.* 131:15904–8
207. Zhang W, Hong M, Luo J. 2020. Halide double perovskite ferroelectrics. *Angew. Chem. Int. Ed.* 59:9305–8
208. Castro-Castro LM, Guloy AM. 2003. Organic-based layered perovskites of mixed-valent gold(I)/gold(III) iodides. *Angew. Chem. Int. Ed.* 42:2771–74
209. Yao Y, Kou B, Peng Y, Wu Z, Li L, et al. 2020. $(C_3H_9NI)_4AgBiI_8$: a direct-bandgap layered double perovskite based on a short-chain spacer cation for light absorption. *Chem. Commun.* 56:3206–9
210. Lassoued MS, Bi LY, Wu Z, Zhou G, Zheng YZ. 2020. Piperidine-induced switching of the direct band gaps of Ag(I)/Bi(III) bimetallic iodide double perovskites. *J. Mater. Chem. C* 8:5349–54

211. Sheng R, Ho-Baillie A, Huang S, Chen S, Wen X, et al. 2015. Methylammonium lead bromide perovskite-based solar cells by vapor-assisted deposition. *J. Phys. Chem. C* 119:3545–49
212. Evans HA, Schueller EC, Smock SR, Wu G, Seshadri R, Wudl F. 2017. Perovskite-related hybrid noble metal iodides: formamidinium platinum iodide [$(FA)_2Pt^{IV}I_6$] and mixed-valence methylammonium gold iodide [$(MA)_2Au^{I}Au^{III}I_6$]. *Inorg. Chim. Acta* 468:280–84
213. Wei F, Deng Z, Sun S, Zhang F, Evans DM, et al. 2017. Synthesis and properties of a lead-free hybrid double perovskite: $(CH_3NH_3)_2AgBiBr_6$. *Chem. Mater.* 29:1089–94
214. Tran TT, Panella JR, Chamorro JR, Morey JR, McQueen TM. 2017. Designing indirect–direct bandgap transitions in double perovskites. *Mater. Horiz.* 4:688–93
215. Evans HA, Wu Y, Seshadri R, Cheetham AK. 2020. Perovskite-related ReO_3-type structures. *Nat. Rev. Mater.* 5:196–213
216. Yu Y, Shang R, Chen S, Wang BW, Wang ZM, Gao S. 2017. A series of bimetallic ammonium AlNa formates. *Chem. Eur. J.* 23:9857–71
217. Kieslich G, Forse AC, Sun S, Butler KT, Kumagai S, et al. 2016. Role of amine–cavity interactions in determining the structure and mechanical properties of the ferroelectric hybrid perovskite $[NH_3NH_2]Zn(HCOO)_3$. *Chem. Mater.* 28:312–17
218. Wu Y, Shaker S, Brivio F, Murugavel R, Bristowe PD, Cheetham AK. 2017. $[Am]Mn(H_2POO)_3$: a new family of hybrid perovskites based on the hypophosphite ligand. *J. Am. Chem. Soc.* 139:16999–7002
219. Evans HA, Deng Z, Collings IE, Wu Y, Andrews JL, et al. 2019. Polymorphism in $M(H_2PO_2)_3$ (M = V, Al, Ga) compounds with the perovskite-related ReO_3 structure. *Chem. Commun.* 55:2964–67
220. Chen S, Shang R, Wang BW, Wang ZM, Gao S. 2018. Electric and magnetic transitions with 90° turning of polarizations in a layered perovskite of $[NH_4Cl]_2$ $[Ni(HCOO)_2$ $(NH_3)_2]$. *APL Mater.* 6:114205
221. Shi C, Ye L, Gong ZX, Ma JJ, Wang QW, et al. 2020. Two-dimensional organic–inorganic hybrid rare-earth double perovskite ferroelectrics. *J. Am. Chem. Soc.* 142:545–51

Annual Review of Materials Research

Volume 51, 2021

Contents

Current Interest

Indexes

Errata

An online log of corrections to *Annual Review of Materials Research* articles may be found at http://www.annualreviews.org/errata/matsci